

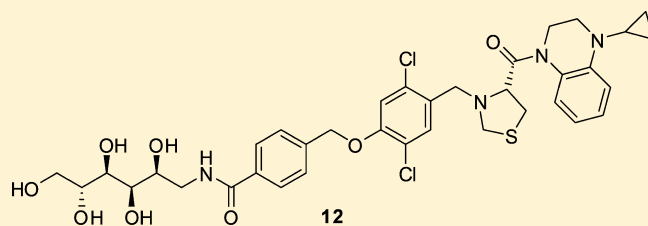
Design of Gut-Restricted Thiazolidine Agonists of G Protein-Coupled Bile Acid Receptor 1 (GPBAR1, TGR5)

Tao Chen, Nicholas William Reich, Noah Bell, Patricia D. Finn, David Rodriguez, Jill Kohler, Kenji Kozuka, Limin He, Andrew G. Spencer,[†] Dominique Charmot, Marc Navre,[‡] Christopher W. Carreras, Samantha Koo-McCoy, Jocelyn Tabora, Jeremy S. Caldwell, Jeffrey W. Jacobs, and Jason Gustaf Lewis^{*†}

Ardelyx, Inc., 34175 Ardenwood Blvd, Fremont, California 94555, United States

Supporting Information

ABSTRACT: Bile acid signaling and metabolism in the gastrointestinal tract have wide-ranging influences on systemic disease. G protein-coupled bile acid receptor 1 (GPBAR1, TGR5) is one of the major effectors in bile acid sensing, with demonstrated influence on metabolic, inflammatory, and proliferative processes. The pharmacologic utility of TGR5 agonists has been limited by systemic target-related effects such as excessive gallbladder filling and blockade of gallbladder emptying. Gut-restricted TGR5 agonists, however, have the potential to avoid these side effects and consequently be developed into drugs with acceptable safety profiles. We describe the discovery and optimization of a series of gut-restricted TGR5 agonists that elicit a potent response in mice, with minimal gallbladder-related effects. The series includes **12** (TGR5 EC₅₀: human, 143 nM; mouse, 1.2 nM), a compound with minimal systemic availability that may have therapeutic value to patients with type 2 diabetes mellitus, nonalcoholic steatohepatitis, or inflammatory bowel disease.



Human TGR5 EC₅₀, 143 nM
Mouse TGR5 EC₅₀, 1.2 nM
Mouse systemic plasma AUC, < 5 ng·h/mL
Mouse fecal recovery, 83 ± 2.6% of dose
Mouse gallbladder (plus bile) recovery, < 0.01% of dose

INTRODUCTION

Bile acid (BA) signaling and metabolism in the gastrointestinal tract plays an important role in the integrated regulation of lipid, glucose, and energy metabolism.¹ Disorders in BA metabolism can cause wide ranging effects including cholestatic liver diseases, dyslipidemia, fatty liver diseases, cardiovascular diseases, and type 2 diabetes mellitus.¹ G protein-coupled BA receptor 1 (GPBAR1), also known as TGR5 (Takeda G protein-coupled receptor 5), is a membrane-based receptor expressed in a broad range of tissue types.^{2–4} In intestinal L cells, a type of enteroendocrine cell present in the distal jejunum, ileum, and colon, TGR5 activation in response to BAs in the gut leads to production and release of incretin hormones including glucagon-like peptides 1 and 2 (GLP-1 and GLP-2).^{5,6} GLP-1 exerts a number of actions that are important for regulating glucose homeostasis,⁷ and GLP-2 is of particular importance to gastrointestinal health.⁸

A major action of GLP-1 occurs in the pancreas, where it enhances glucose-stimulated insulin production and release and glucose sensitivity in β cells.⁷ GLP-1 analogs have proven utility in the treatment of patients with type 2 diabetes mellitus.^{9,10} GLP-1 also has extra-pancreatic effects that may make a GLP-1-based therapy an attractive option for treating nonalcoholic steatohepatitis (NASH), a severe form of nonalcoholic fatty liver disease (NAFLD). NASH is charac-

terized by steatosis, an excessive accumulation of hepatic fat, together with evidence of hepatocyte injury and inflammation, steatohepatitis, and fibrosis.¹¹ Insulin resistance in liver and adipose tissue, as well as excessive hepatic lipogenesis, are believed to be important in the pathogenesis of NAFLD/NASH.^{12–14} Studies in animal models of NASH have shown that GLP-1 therapy improves insulin sensitivity and reduces hepatic glucose production, and can reduce hepatic steatosis, inflammation, steatohepatitis, and fibrosis.^{15–18} In patients with NASH, a placebo-controlled study found that the GLP-1 analog liraglutide promoted histological resolution of NASH, as well as reductions in body weight, plasma fasting glucose, and glycosylated hemoglobin levels.¹⁹ Studies in a subset of patients from this clinical trial revealed that liraglutide increased hepatic and adipose tissue insulin sensitivity and reduced hepatic de novo lipogenesis and inflammatory biomarker levels.²⁰ GLP-2, which is also released in response to TGR5 agonism, has anti-inflammatory properties²¹ and has been shown to accelerate liver regeneration in mice following partial hepatectomy when administered exogenously.²² Thus, stimulation of GLP-1 and GLP-2 production by TGR5

Received: February 23, 2018

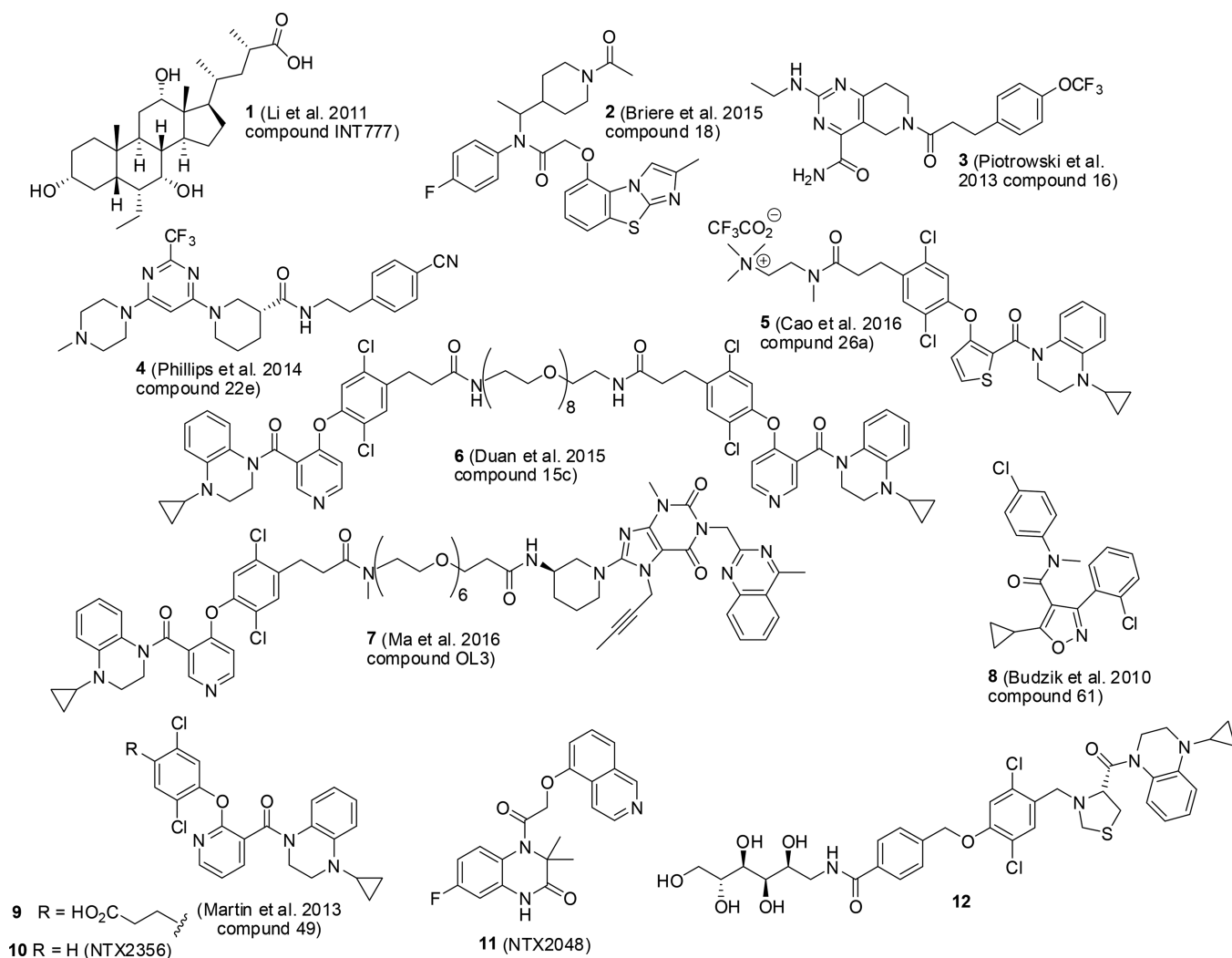


Figure 1. Known TGR5 agonists and structure of compound 12. References: Li et al. 2011,³³ Briere et al. 2015,³⁵ Piotrowski et al. 2013,³⁶ Phillips et al. 2014,³⁷ Cao et al. 2016,³⁸ Duan et al. 2015,³⁹ Mat et al. 2016,⁴⁰ Budzik et al. 2010,⁴² Martin et al. 2013,⁴³ and Ito et al. 2006.⁴³

agonists may be of therapeutic benefit in patients with metabolic diseases such as NAFLD/NASH.^{23,24}

In the intestine, GLP-2 has multiple effects including expansion of the mucosal surface area through stimulation of crypt cell proliferation and enhancement of nutrient digestion and absorption.⁸ The actions of GLP-2 on the intestine have been translated into products with therapeutic potential. For example, a long-acting GLP-2 analog, teduglutide, increases cell proliferation in the gut and has been approved for the treatment of short bowel syndrome.^{25,26} TGR5 agonism also has anti-inflammatory effects *in vitro* and *in vivo*.^{27–29} In mouse models of colitis, TGR5 agonists modulate the integrity of the intestinal barrier and ameliorate disease activity.^{30,31} This combination of proliferative and anti-inflammatory effects in response to TGR5 agonism in the intestine may prove to be efficacious in the treatment of patients with inflammatory bowel disease (IBD) in which a complex interaction of environmental, genetic, and immunoregulatory factors trigger an autoimmune response against elements of the gastrointestinal tract, resulting in tissue inflammation and lesions.³²

A selection of known TGR5 agonists 1–11 is shown in Figure 1. Although TGR5 is an attractive therapeutic target, TGR5 agonists have historically been associated with undesirable side effects. TGR5 is highly expressed in the

gallbladder, where activation of the receptor stimulates its filling with bile and blocks its emptying in response to a meal.^{33,34} Systemic TGR5 agonism therefore poses the risk of stimulating excessive gallbladder filling combined with preventing complete gallbladder emptying, which can lead to gallstone formation. Indeed, assays in mice have shown that TGR5 activation in the epithelium of the gallbladder by administration of BA derivatives (e.g., INT-777, Intercept Pharmaceuticals, 1)³³ or other small-molecule TGR5 agonists (e.g., compound 18, Eli Lilly, 2)³⁵ causes increased gallbladder filling and blockade of emptying. In addition, several systemically available TGR5 agonists (e.g., Pfizer compound 16, a tetrahydropyrido[4,3-*d*]pyrimidine amide, 3;³⁶ Novartis compound 22e, a (*R*)-*N*-(4-cyanophenethyl)-1-(2-methyl-6-(4-methylpiperazin-1-yl)pyrimidin-4-yl)piperidine-3-carboxamide, 4³⁷) have been shown to change heart rate and blood pressure in dogs. The design of therapeutic molecules targeting TGR5 in the gut that are not absorbed into the bloodstream, yet are capable of eliciting the desired basolateral secretion of incretins, is an attractive approach to limiting the systemic target-based risk. Recently, intestine-targeted TGR5 agonists 5–7 have been identified that normalize blood glucose in mouse models, with reduced gallbladder-based side effects versus absorbed TGR5 agonists.^{38–40} Differing strategies were

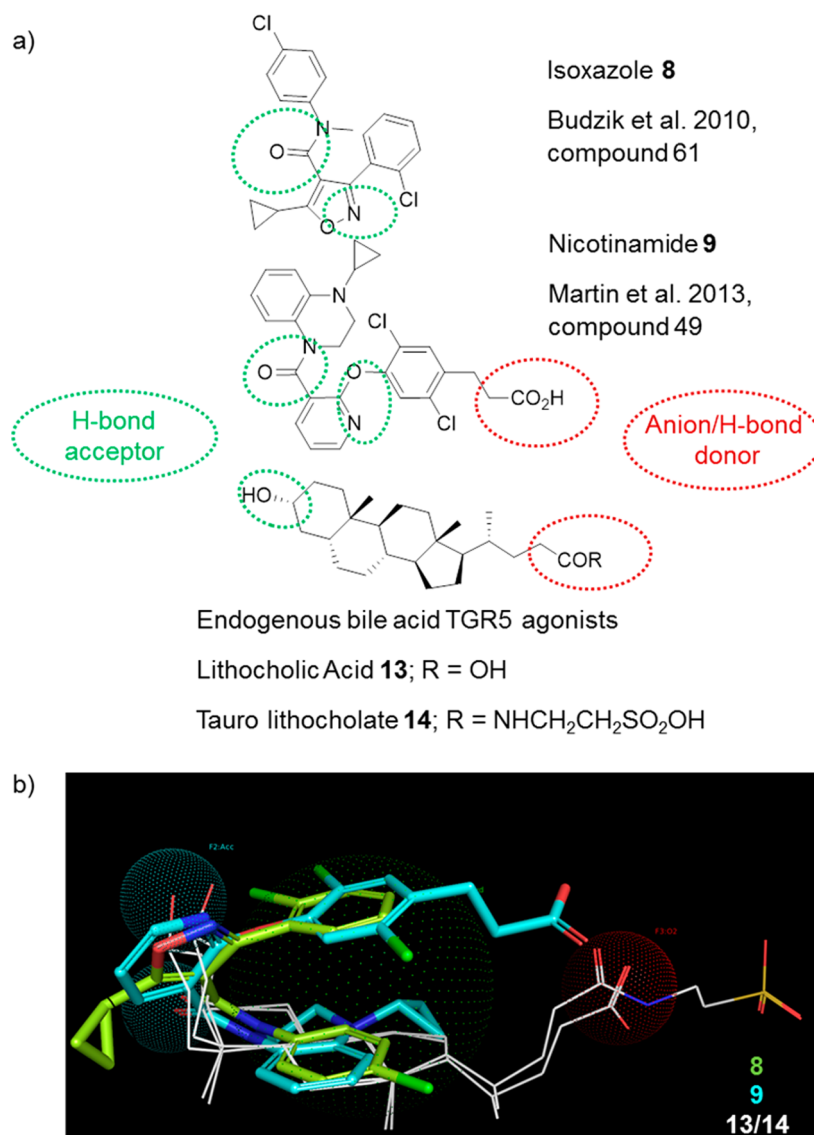


Figure 2. TGR5 agonists. (a) Examples of aryl amide and endogenous TGR5 agonists. (b) Alignment of chemotype examples. References: Budzik et al. 2010⁴² and Martin et al. 2013.⁴³

used to minimize systemic exposure, including cationic functionality, dimerization, and high molecular weight, with gut restriction achieved to varying degrees of success. Examples of strategies for intestinal targeting of drugs have been reviewed,⁴¹ with minimal absorption of the drug by virtue of its physical properties being a particularly attractive strategy where the target is accessible from the gastrointestinal lumen. The performance, structural requirements and physical characteristics of such minimally systemic compounds is a relatively unexplored field of medicinal chemistry.

We describe the discovery and optimization of a series of gut-restricted selective thiazolidine TGR5 agonists that elicit a potent response with minimal gallbladder-related effects. The series includes **12** (Figure 1), a compound with minimal systemic availability that may have potential therapeutic value to patients with type 2 diabetes mellitus, NAFLD/NASH, or IBD.

RESULTS

Pharmacophore Model Generation. Our evaluation of disclosed small-molecule TGR5 agonists in the literature led to

a hypothesis that aryl amide chemotype molecules, such as the isooxazole **8** and the nicotinamide **9** (Figure 2a),^{42,43} bind to the same site on the TGR5 receptor as endogenous BA ligands, lithocholic acid **13**, and tauro lithocholate **14** (Figure 2a). All of these molecules contain cyclic hydrophobic moieties with hydrogen bond acceptors in close proximity. We predicted that the side chain of the BAs could define a potential solvent-accessible region, which could be exploited to increase the binding affinity of a novel TGR5 agonist over endogenous BAs.

To explore this hypothesis further, we prepared a structure–activity relationship (SAR)-guided shape-based conformer alignment of the endogenous BAs, **13** and **14**, with **8** and **9** (Figure 2b). We noted that the lowest energy conformers of **8** and **9** have common features. First, the 1-hydroxyls of BAs align with H-bond acceptors in **8** and **9**. Second, the 4-position carboxylate of **9** extends toward the BA side chains in a “vector to solvent” manner. Finally, the central heterocycles of **8** and **9** constrain the aryl hydrophobic moieties of the two molecules. The central heterocycle and aryl hydrophobic moieties then align with the steroid core moiety of the BAs.

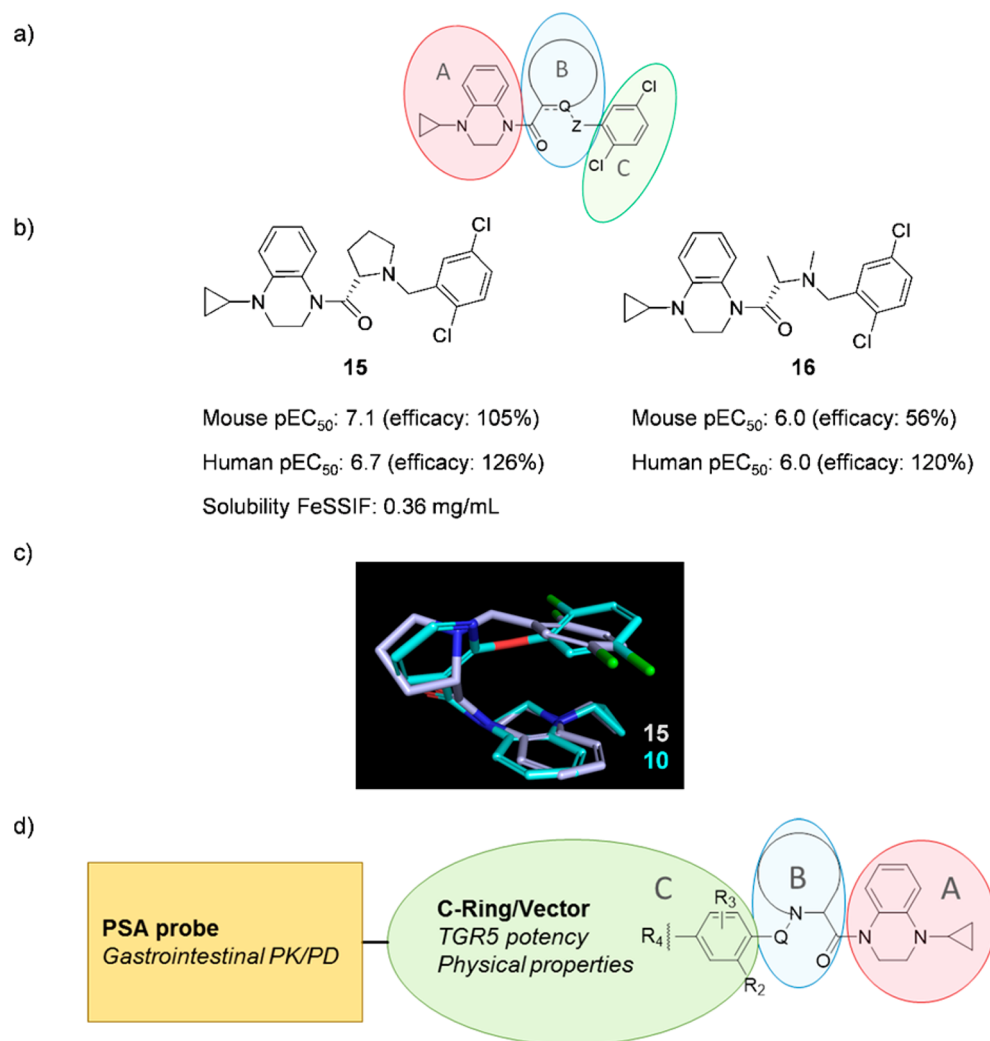


Figure 3. Generation of a gut-restricted TGR5 agonist pharmacophore. (a) Initial pharmacophore for the TGR5 agonist. (b) Early hits **15** and **16**. (c) Alignment of **10** (nicotinamide **9** with propanoic acid vector group removed) and **15** low energy conformers. (d) Gut-restricted pharmacophore variant: the C-ring/vector region and PSA probe moiety facilitate optimization of properties such as solubility, stability, and membrane permeability, as well as receptor binding affinity.

A pharmacophore model was developed for a novel TGR5 agonist, based on core features of **9** (Figure 3a). The pharmacophore was divided into three fragments for the purpose of exploring SARs: the quinoxaline moiety (A-ring), the central heterocycle (B-ring), and the 2,5-dichlorobenzene moiety (C-ring).

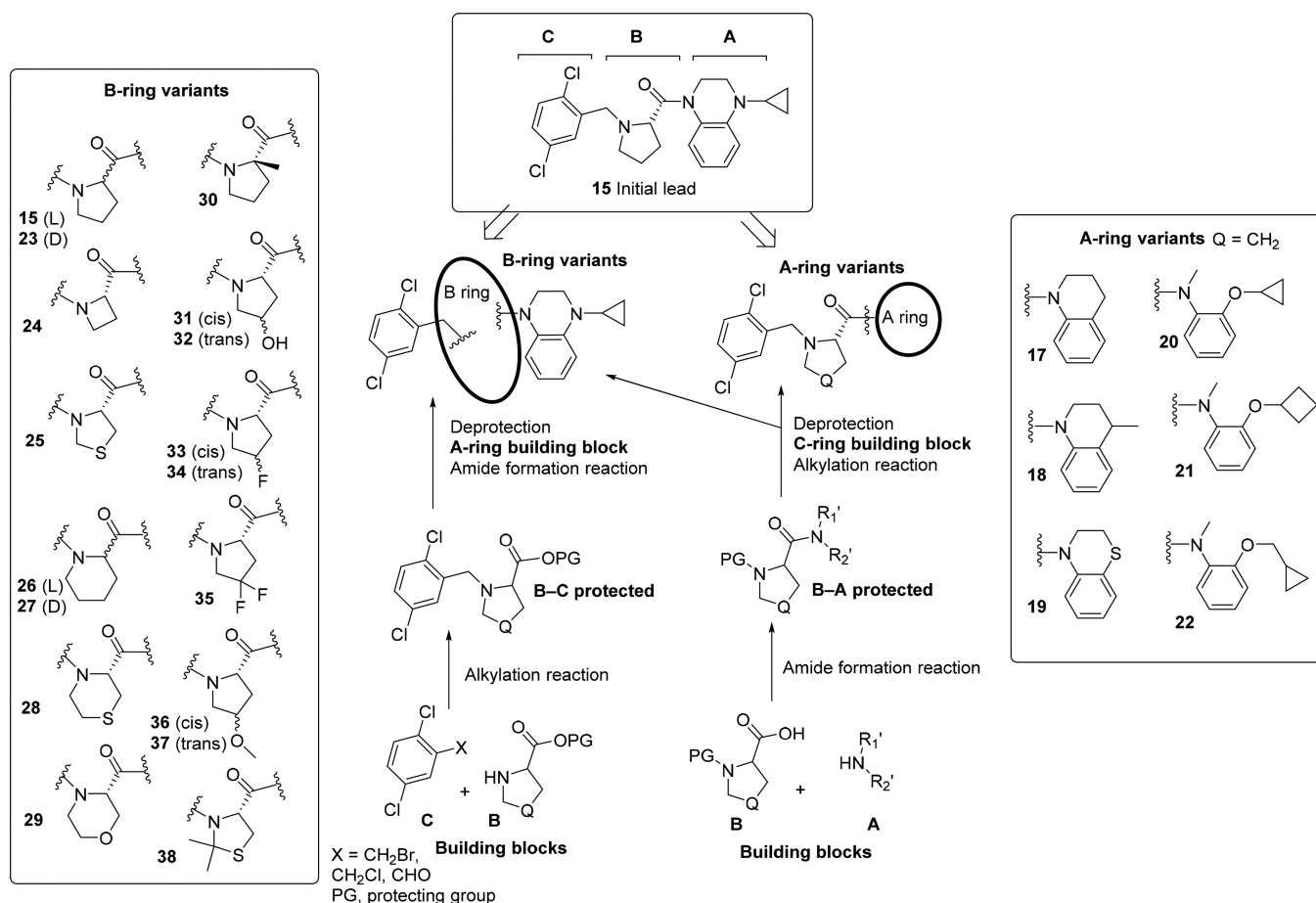
Design Approach. As a first step toward identifying a suitable starting compound, nonaryl options for the central B-ring were surveyed in the context of A- and C-rings that matched the pharmacophore. Early hit **15**, based on L-proline, provided a constructive constraint for the pharmacophore relative to compounds with acyclic amino acids in the B-ring position, such as **16** (Figure 3b). In addition, the potency (pEC₅₀) and efficacy of **15** at the TGR5 receptor were higher than those of **16** (efficacy was assessed relative to reported TGR5 agonist **11**,⁴⁴ Figure 1), providing support for a bulkier constrained cyclic motif in this region. An alignment of low energy conformers of **15** with **10** (where **10** represents nicotinamide **9** with the propanoic acid vector group removed) demonstrated the similarity of **15** to **9** (Figure 3c).

Compound **15** was selected for further optimization based on the vast pool of available cyclic amino acid diversity that

provided the opportunity to fine-tune B-ring electronics and sterics and its physical property advantages over the relatively hydrophobic nicotinamide analog **10**. The solubility of **15** in fed state simulated intestinal fluid (FeSSIF)⁴⁵ was found to be 0.36 mg/mL, whereas **10** was found to be insoluble in FeSSIF (<0.05 mg/mL); cLogP values were 4.92 and 5.42, respectively. The heterocycloalkane B-ring of **15** was also advantageous over the aryl B-ring of **10**, as limiting aryl ring count to no more than three in candidate compounds has predictive value for successful drug development.⁴⁶

Our hit-to-lead approach was to tune **15** for optimal performance as a gut-acting, minimally absorbed TGR5 agonist (Figure 3d). After exploring options to optimize the A-ring, we planned to survey options for the B-ring with the aim of identifying constraints that would best enable exploration of SAR at the C-ring 4-position. The C-ring could be manipulated to optimize ligand performance properties, including solubility and stability in the gastrointestinal tract. Probing the SAR of a vector extending from the 4-position could then enable incorporation of functionality to optimize in vivo pharmacokinetic/pharmacodynamic (PK/PD) performance, as well as fine-tuning target potency.

Scheme 1. Generalized Retrosynthetic Analysis of Production of A- and B-ring Variants of Substituted Thiazolidine TGR5 Agonists



The broad concept of the kinetophore, defined as a structural unit violating Lipinski's rule of five⁴⁷ in order to restrict permeability, is known.⁴⁸ However, the specific structural attributes required to achieve desired PK and PD performance in the luminal environment of the intestine, including the relationship between structure and target binding in the context of chyme, mucus, regional pH gradients, and transit time, have not been systematically investigated. Furthermore, appropriate kinetophores must not only limit passive permeation but also limit facilitated uptake via transporters such as ileal bile acid transporter (IBAT), which have broad substrate specificity.⁴⁹ We evaluated the relationships between kinetophore attributes, overall physical properties, and in vivo performance in a homologous series of TGR5 agonist ligands.

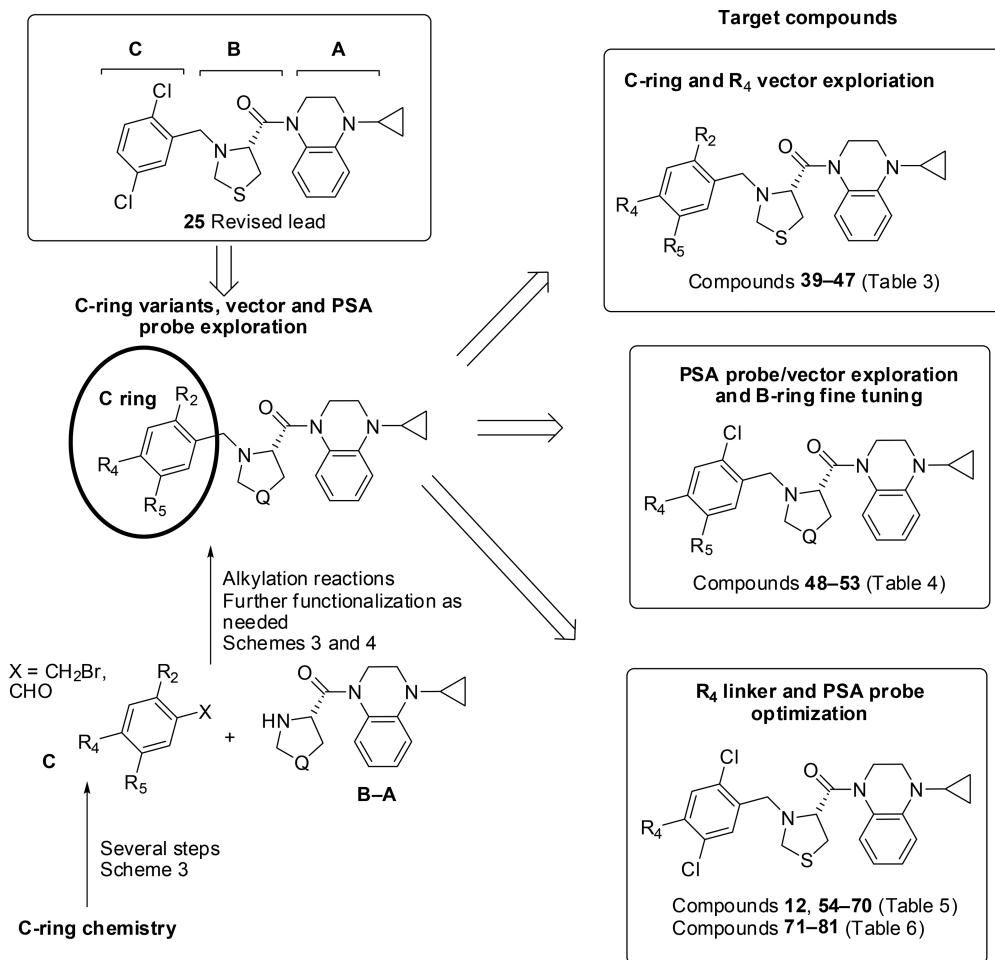
Chemistry. A general synthetic route for the preparation of a comprehensive set of analogs of the TGR5 agonists, with varied functionality in the A, B, and C rings of the designed pharmacophore, is provided in Schemes 1 and 2.

A-ring building blocks used were prepared via procedures detailed in the Supporting Information or were commercially available materials. B-ring variants were introduced by utilizing a range of 4–6-membered heterocyclic amino acids with differing heteroatom and ring substituent composition. A-ring building blocks were coupled with N-protected B-ring carboxylic acid building blocks to produce N-protected B–A amide adducts (Scheme 1). These were deprotected to produce the free amines that were subsequently coupled with

benzylhalides or benzaldehydes as C-ring building blocks, via nucleophilic substitution or reduction amination reactions, respectively, to produce the C–B–A adducts. In producing some of the B-ring variants, the carboxylate protected B-ring building block was coupled directly with the C-ring building block to produce protected B–C adducts; these were deprotected to produce the free carboxylic acids that were coupled with the amino groups of the A-ring building blocks in amide formation reactions to produce the C–B–A adducts. Following this general approach, the A-ring variants 17–22 (Table 1) and B-ring variants 23–38 (Table 2) were produced (Supporting Information).

A similar general approach as that outlined above for the production of A-ring and B-ring variants was used for the production of C-ring variants 12 and 39–81 (Tables 3–6), in which 25 served as a “revised lead” compound (Scheme 2). In order to optimize target interaction in the vector to solvent region of the C-ring, we developed chemistry that allowed rapid production of diverse functionality on the C-ring, predominantly in the R₄-position, favored by our pharmacophore model (Schemes 3 and 4). Selective Friedel–Crafts formylation of 2,5-dichloro-4-methoxybenzene to generate benzaldehyde 82 followed by nucleophilic deprotection of the 4-hydroxy group provided phenol 83. Trifluoromethylsulfonation of the 4-position provided triflate 84, which served as a versatile starting material for Sonigashira introduction of 4- and 5-carbon alkynes with pendant functionality to produce 85–87. Selective hydrogenation of the R₄ alkyne with rhodium

Scheme 2. Generalized Retrosynthetic Analysis of Production of C-ring Variants of Substituted Thiazolidine TGR5 Agonists



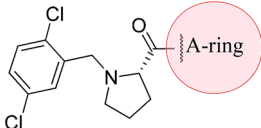
on carbon provided protected 4-alkyl carboxylates and amines **88–90**. 1,4-Dichloro-2,5-dimethylbenzene was used as a starting material to produce dialdehyde **91** via chromium trioxide oxidation, which was subsequently used to produce the 3-carbon variant in the 4-position, obtained by Wittig homologation of **91** to produce alkene **92** followed by catalytic hydrogenation to **93**. The 3-carbon variant in the 5-position was obtained by Heck coupling of *t*-butyl acrylate with 4-chloro-5-(hydroxymethyl)bromobenzene to produce **94**, which was hydrogenated to **95** and converted to the benzyl bromide **96**.

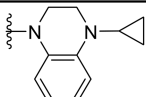
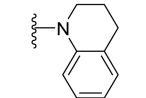
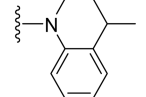
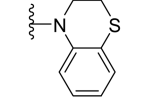
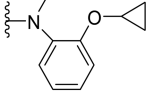
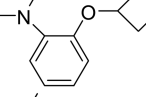
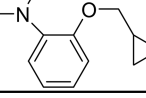
In parallel, B–A ring constructs were synthesized for coupling with the C-ring variants (Scheme 3). 1-Cyclopropyl-1,2,3,4-tetrahydroquinoxaline was coupled with the *N*-Boc-protected cyclic amino acid **97**, resulting in the *N*-protected B–A adduct **98**, which was deprotected under acidic conditions to produce **99**. Key intermediate **99** was coupled with aldehydes **83**, **88–91**, and **93**, via reductive amination reactions to produce intermediates **42**, **46**, and **100–103**, while benzyl bromide **96** was coupled with **99** via a nucleophilic substitution reaction resulting in **104**. Compounds **100–104** were deprotected to produce carboxylic acids **105**, **45**, and **107** and amines **106** and **44** for vector exploration (Scheme 4). Phenol **42** and benzyl alcohol **46** were further functionalized to produce aromatic carboxylic acid intermediates including **43** and **47**, with their aryl groups serving as linkers. The carboxylic acids **105**, **45**, **43**, **47**, and

107 and amine analogs **106** and **44**, subsequently served as key intermediates with anchor points for incorporation of *D*-glucamine and other functionality via urea- and amide-forming chemistry for vector and PK property exploration, producing compounds such as the amides **12**, **50–54**, **61**, and **70** and the ureas **64**, **65**, and **67–69** (Scheme 4). All other analogs tested were produced via similar chemistry, as outlined in the Supporting Information.

A-ring Optimization. To explore options for the A-ring, a series of over 30 compounds with inactive A-ring amides were tested, including both cyclic and acyclic moieties (selected compounds, **17–22**, shown in Table 1). None of the compounds in this series was found to have improved activity over **15** at the TGR5 receptor.

Options assessed for cyclic moieties were substitution of the 1,2,3,4-tetrahydroquinoxaline moiety for 1,2,3,4-tetrahydroquinoline **17** or 3,4-dihydro-1,4-benzothiazine **19**, both of which retained some activity, or substitution of the 4-*N*-cyclopropyl group for methyl **18**, which had no activity. Acyclic moieties were also assessed, with the piperazine ring of the 1,2,3,4-tetrahydroquinoxaline moiety opened up by removal of the 3-position carbon. The 4-*N*-cyclopropane group was substituted for 4-*O*-cyclopropane **20** or 4-*O*-cyclobutane **21**, both of which retained some activity, or 4-*O*-methyl-cyclopropane **22**, which had no activity. It appeared that a 1,2,3,4-tetrahydroquinoxaline A-ring was privileged for potent TGR5 activity.

Table 1. SAR of Selected Compounds from A-ring Amide Series^a


Compound	A-ring	TGR5 mouse		TGR5 human	
		pEC ₅₀	Efficacy (%)	pEC ₅₀	Efficacy (%)
15		7.0	105	6.7	126
17		5.6	78	5.1	129
18		< 5.0	ND	< 5.0	ND
19		5.3	65	5.4	69
20		6.0	75	6.0	98
21		6.0	100	6.1	120
22		< 5.0	ND	< 5.0	ND

^aData are means of duplicate experiments.

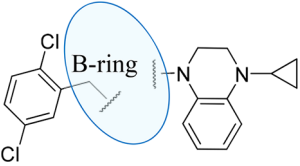
B-ring Optimization. A series of analogs of **15** and **23–38** explored the effects of different steric and electronic options in the B-ring of the molecule (Table 2). The D-proline form of **15**, **23**, had reduced potency at both mouse and human TGR5 versus the L-proline form **15**. Contraction of the **15** pyrrolidine ring to azetidine **24** reduced activity, as did expansion to piperidine, particularly the D-form of the molecule (L-form **26**, D-form **27**). L-Form B-rings were therefore retained for further compounds in the series. A thiazolidine analog of **15** and **25** was found to improve activity both overall and in terms of parity at the mouse versus human TGR5 receptors. Expansion of the thiazolidine ring of **25** to thiomorpholine **28** or substitution for morpholine **29** reduced activity, providing further evidence that 5-membered B-rings were optimal. A 2-methyl-pyrrolidine ring **30** reduced activity. Substitutions at the 4-position of **15** were then assessed. Of 4-hydroxy- (*cis* **31**, *trans* **32**), 4-fluoro- (*cis* **33**, *trans* **34**), 4-difluoro- (**35**) and 4-methoxy- (*cis* **36**, *trans* **37**) substituted compounds, only the 4-fluoro-substituted compounds, particularly **33**, had increased activity over **15**. Finally, a 5-dimethyl analog of **25**, **38**, had reduced activity.

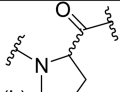

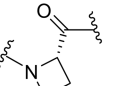
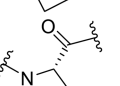
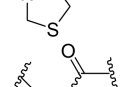
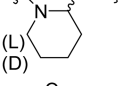
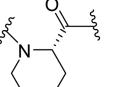
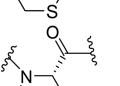
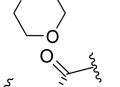
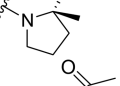
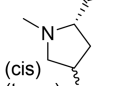
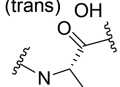
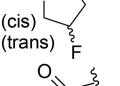
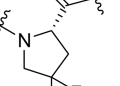
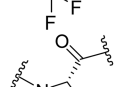
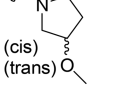
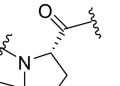
In summary, B-ring thiazolidine **25** and *cis*-4-fluoroproline **33** had increased activity over **15**, both overall and in terms of parity at the mouse versus human TGR5 receptor. It was

concluded from analysis of this series that ring size and amine p*K*_a, as determined by the electronegativity of the atom(s) at position 4, were both key variables for activity.

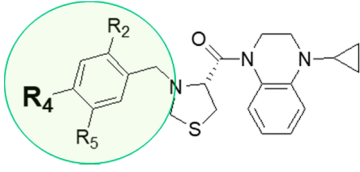
C-ring and Vector Optimization. Our next step was to optimize the C-ring, using **25**, with the thiazolidine B-ring, as the parent ligand. Substitutions at the 2-, 4-, and 5-positions were assessed (Table 3). Among substitutions at the 2- and 5-positions, an R₂, R₅ dichloro C-ring (i.e., **25**) retained the best activity in this thiazolidine chemotype. An R₂ trifluoromethyl substitution of **25**, **39**, resulted in slightly reduced activity. Iodo (**40**) and cyclopropyl (**41**) substitutions at R₅ also led to reduced activity.

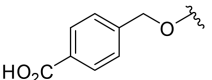
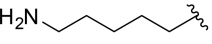
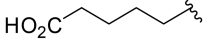
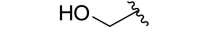
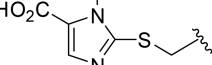
Our strategy for probing SAR at R₄, the 4-position of the C-ring, allowed us rapid access to diverse vectors (Schemes 3 and 4). Vector length (of 1 to 6 or more atoms), constraint, and polarity could all be manipulated, and terminal functionalities such as hydroxyl, carboxylate, and amine groups could be readily appended. The R₄ position was found to tolerate extended vectors, with extensions at this position producing compounds that largely retained or improved activity (**43–47**; Table 3). Of note, carboxylic acid derivative (**45**) and alcohol derivative (**46**) R₄ groups increased mouse TGR5 activity. The terminal group of the R₄ vectors in compounds **43–47** (carboxylic acid, amine, alcohol) also presented chemistry

Table 2. SAR of B-ring Series^a


Compound	B-ring	TGR5 mouse		TGR5 human	
		pEC ₅₀	Efficacy (%)	pEC ₅₀	Efficacy (%)
15		7.0	105	6.7	126
23	15 (L) 23 (D) 	5.9	77	5.6	122
24		6.2	77	6.0	106
25		7.6	97	7.6	116
26		5.7	40	5.8	70
27	26 (L) 27 (D) 	< 5.5	43	5.7	64
28		5.8	58	6.5	67
29		6.5	86	6.6	111
30		5.9	51	6.0	35
31		6.4	72	6.1	95
32	31 (cis) 32 (trans) 	6.6	72	6.8	146
33		7.3	78	7.3	110
34	33 (cis) 34 (trans) 	7.0	90	7.2	147
35		6.9	98	6.9	115
36		6.5	72	6.7	128
37	36 (cis) 37 (trans) 	7.0	96	6.9	177
38		6.4	62	6.6	106

^aData are means of duplicate experiments.

Table 3. SAR of C-ring and R₄ Vector Series^a


Compound	R ₄	R ₅	R ₂	TGR5 mouse		TGR5 human	
				pEC ₅₀	Efficacy (%)	pEC ₅₀	Efficacy (%)
25	H	Cl	Cl	7.6	97	7.6	116
39	H	Cl	CF ₃	7.2	112	7.4	154
40	H	I	Cl	6.9	92	6.9	90
41	H	cPr	Cl	6.1	178	6.3	136
42	OH	Cl	Cl	7.8	108	7.0	103
43		Cl	Cl	7.5	121	6.4	89
44		Cl	Cl	7.2	98	6.7	144
45		Cl	Cl	8.0	76	7.3	88
46		Cl	Cl	8.2	83	7.6	129
47		Cl	Cl	8.0	89	6.5	138

^aData are means of duplicate experiments.

opportunities to append kinetophores to modify PK and performance.

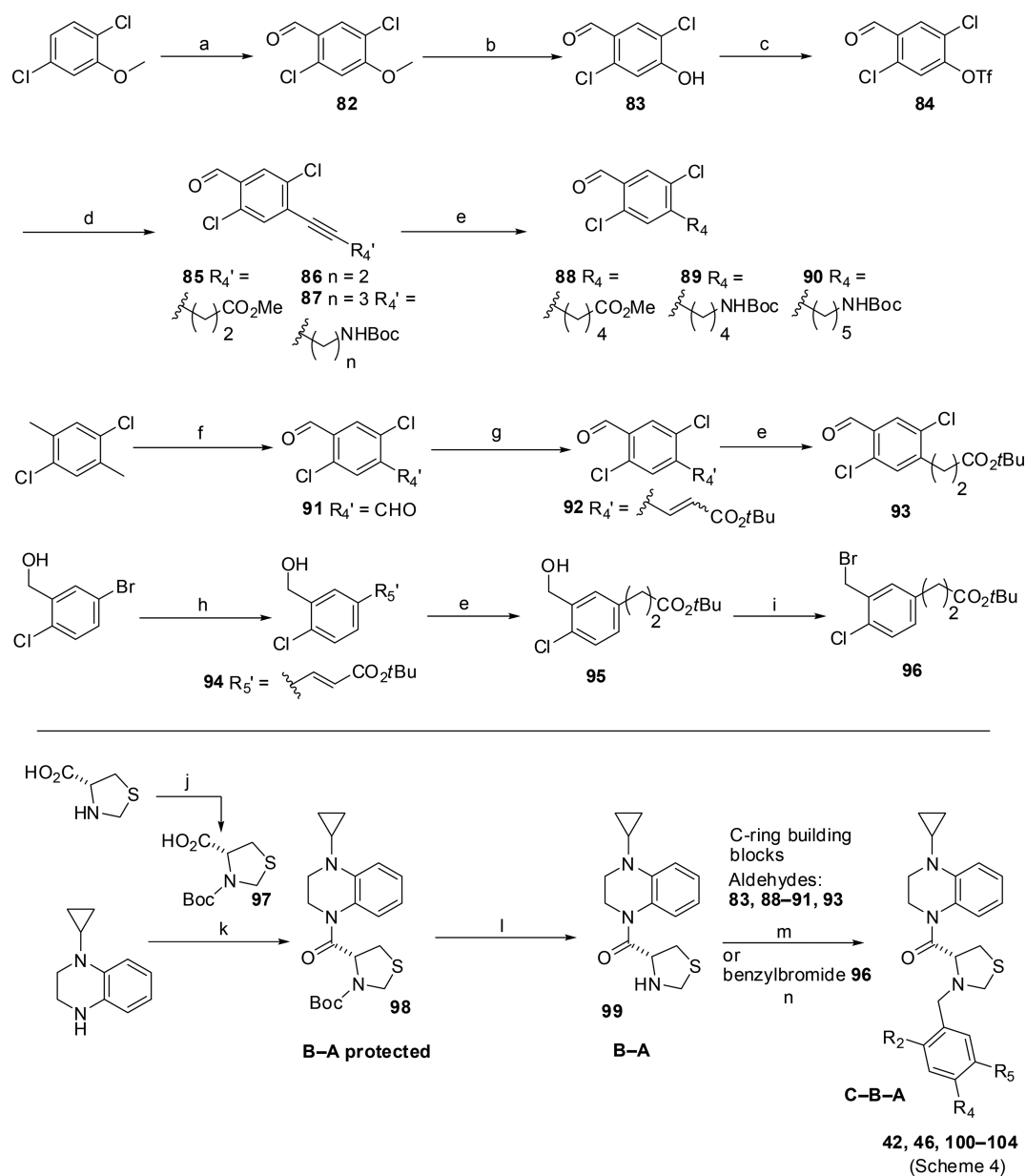
At this stage, there were several unknowns regarding the R₄ vector that required investigation and optimization, specifically: (1) what changes to polar surface area (PSA) could be incorporated while retaining activity?; (2) could additional distal binding interactions be made with the TGR5 receptor by extending the R₄ vector?; (3) which PSA characteristics affect PK/PD profiles?

As a first step toward answering these questions, we assessed a series of compounds based on **25**, with extended vectors at R₄ as PSA probes, in combination with variants at the 4-position of the B-ring (Table 4). R₄ extended as D-glucamide (**50**) increased mouse and maintained human TGR5 potency relative to parent ligand **25**. A thiazolidine B-ring (**25**) was favored over proline (**48**) and 4-fluoroproline (**49**) when the R₄ vector was extended as D-glucamide, whereas R₅ extended as D-glucamide (**51**) was not favorable. N-Methylglucamide R₄ extensions (**52** and **53**) resulted in similar mouse TGR5 activity to **50** but reduced human TGR5 activity. With the R₄ D-glucamide apparently favorable, options were then explored for the section of the R₄ vector linking the C-ring with D-glucamine (Table 5). In addition, other polyol PSA probes with similarity to D-glucamide were assessed at R₄ (Table 5).

Mouse TGR5 activity was enhanced with aryl and heteroaryl R₄ linkers (as in **12** and **61**), but human TGR5 activity was slightly reduced. D-Glucamine with an alkyl amide linker (**64** and **70**) and a tris urea derivative with alkyl linker (**69**) were found to have favorable human and mouse TGR5 activity.

Optimization of In Vivo PK/PD Profile. While optimizing the in vitro activity of our TGR5 agonists we also began to optimize PK/PD performance in vivo. We used a single time point mouse model under fasted conditions to rapidly compare compound performance in terms of GLP-1 secretion and propensity to cause gallbladder filling; under fasted conditions, gallbladder emptying does not occur, and filling is predominant. Male C57Bl/6 mice were administered compounds orally at 30 mg/kg, and serum and gallbladders were collected after 8 h. Gallbladder weight and compound concentration were measured to assess gallbladder filling and local accumulation of TGR5 agonist over the course of the experiment. Simultaneous plasma total GLP-1 (tGLP-1) served as a surrogate for active GLP-1 secreted over the duration of the experiment. Compound concentration in gallbladder tissue and bile (combined) and plasma were also assessed at the same time point.

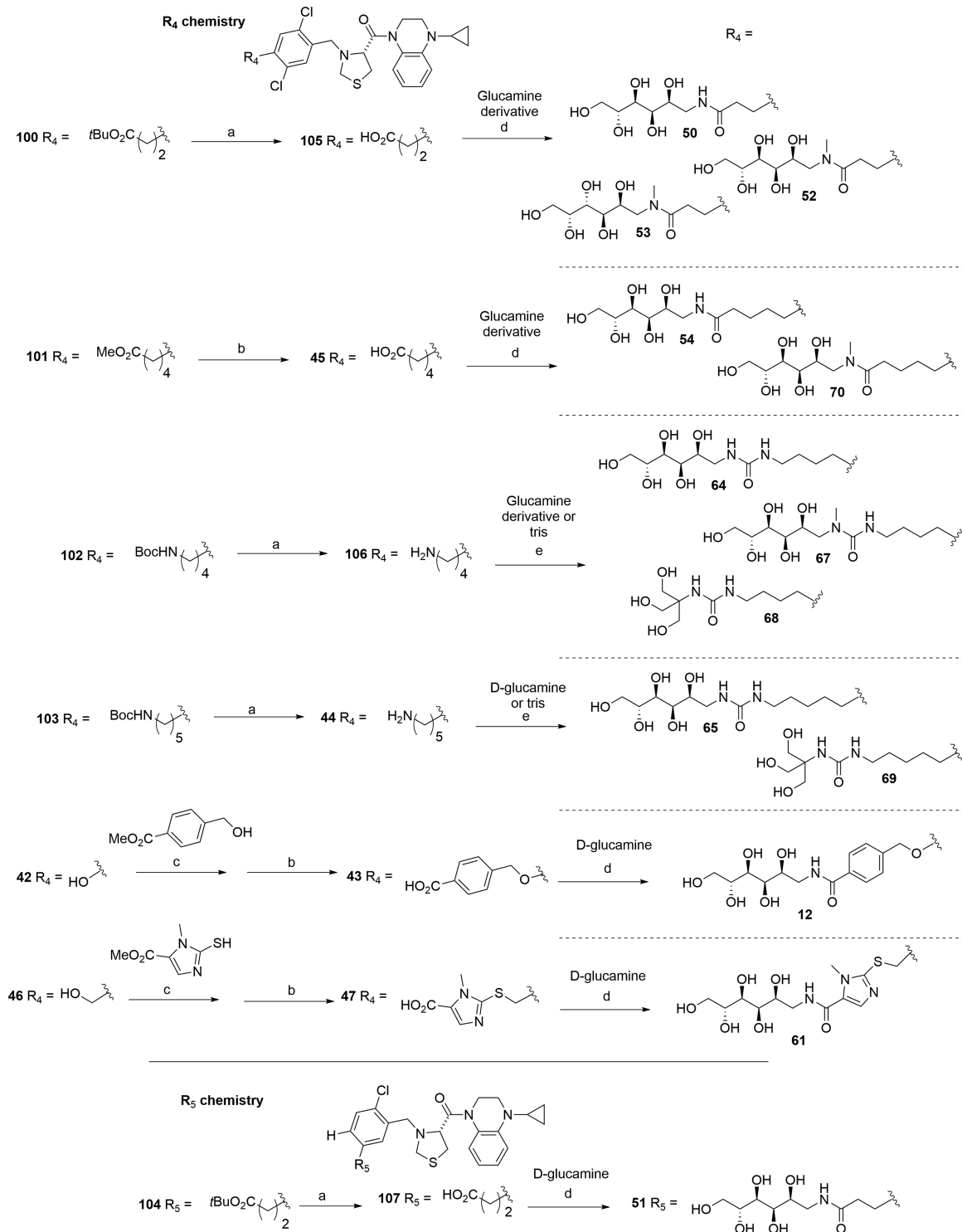
A set of 22 diverse R₄ PSA probe-appended thiazolidine examples were evaluated for PD response (i.e., GLP-1

Scheme 3. Synthesis of Substituted C-Ring Building Blocks and Key B–A-ring Intermediates^a

^aReagents and conditions: (a) MeOCHCl_2 , TiCl_4 , DCM, 0–60 °C 2 h; (b) LiCl , DMF, 140 °C, 16 h; (c) TiF_2O , triethylamine, DCM; (d) $\text{Pd}(\text{PPh}_3)_2\text{Cl}_2$, CuI , DIEA, DMF; (e) Rh/C , H_2 , EtOAc ; (f) CrO_3 , AcOH , Ac_2O , H_2SO_4 , 0–10 °C; (g) $\text{Ph}_3\text{PCH}_2\text{CO}_2\text{tBu}$, $\text{NaOH}_{(\text{aq})}$, DCM; (h) *t*-butyl acrylate, $\text{Pd}(\text{OAc})_2$, PPh_3 , triethylamine; (i) Br_2PPh_3 , acetonitrile; (j) Boc_2O , NaOH , dioxane/water; (k) HATU, DIEA, DMF, rt, 3 h; (l) conc. HCl , dioxane, 0 °C–rt, 1 h; (m) $\text{NaBH}(\text{OAc})_3$, DCE, rt, 1 h; (n) K_2CO_3 , DMF.

secretion and gallbladder filling) and PK. The set consisted of 11 compounds from the D-glucamine amide/urea R_4 vector series (**12**, **50**, **52–54**, **59**, **61**, **64**, **67**, **69**, and **70**), and 11 further compounds to explore more vector options (**71–81**; Table 6). This compound set was designed to explore a range of physical property-based gut-restriction strategies (PSA, charge, and hydrogen bond donors and acceptors); all compounds had potent activity at the mouse TGR5 receptor (pEC_{50} 7.4–9.0). Compounds **52**, **54**, **12**, **64**, and **70** increased plasma levels of tGLP-1 substantially more than vehicle, with little effect on gallbladder weight (Table 6). All five compounds were found at very low concentrations in both gallbladder/bile and plasma.

Analysis of the relationship between the physical properties of this compound set and their in vivo performance identified **12** and **64** as the most suitable candidates for lead compounds. These two compounds produced the highest tGLP-1 induction among the set (**12**, ~4-fold; **64**, ~5-fold), which was found to correspond well with in vitro potency at mouse TGR5 (pEC_{50} : **12**, 8.9; **64**, 8.7; Figure 4a). Relative to the other compounds of the set, **12** and **64** stimulated moderate increases in gallbladder weight (both ~1.7-fold; Figure 4b). In contrast, **69** and **74**, both of which did not contain the glucamine-based R_4 vector, were found to stimulate greater increases in gallbladder weight (2.0–2.5-fold). Calculated values for PSA (both ~170 Å²), hydrogen bond acceptors (**12**, 10; **64**, 9), hydrogen bond donors (**12**, 6; **64**, 7), and molecular weight (**12**, 761.7 g/mol;

Scheme 4. Representative Vector Elaboration Chemistry^a

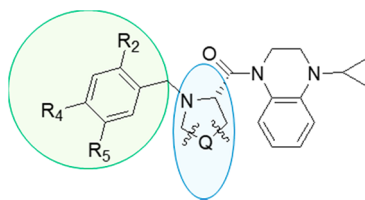
^aReagents and conditions: (a) TFA; (b) LiOH_(aq), dioxane; (c) DIAD, PPh₃, DCM, rt 18 h; (d) HATU, DIEA, DMF; (e) CDI, DIEA, DMF.

64, 726.7 g/mol) suggest 12 and 64 would have minimal potential for passive permeation (Figure 4c, d).

To assess selectivity further, we evaluated activity at other BA targets: farnesoid X receptor (FXR) and IBAT. No activity was detected at up to 50 μM for 12, 64, or the parent compound 25 for human FXR activation⁵⁰ (all pEC₅₀ < 4.3) or inhibition of [³H]taurocholic acid uptake in human or mouse IBAT cellular assays⁵¹ (all pIC₅₀ < 4.6). Compound 12 was

further characterized at 10 μM in an in vitro pharmacology diversity panel (Cerep-Panlabs), binding only three of 80 targets to an extent greater than 80% (see Supporting Information); none of these targets are exposed to the gut lumen.

In Vivo Proof of Concept. Compound 12 had favorable properties for in vivo proof-of-concept as a gut-restricted TGR5 agonist (Table 7). Both plasma and gallbladder

Table 4. SAR of PSA Probe/Vector Series (Part 1)^a

Compound	R ₄	R ₅	R ₂	Q	TGR5 mouse		TGR5 human	
					pEC ₅₀	Efficacy (%)	pEC ₅₀	Efficacy (%)
25	H	Cl	Cl		7.6	97	7.6	116
48		Cl	Cl		6.4	66	6.9	124
49		Cl	Cl		6.2	70	6.4	96
50		Cl	Cl		8.2	106	7.5	174
51	H		Cl		6.8	110	6.1	116
52		Cl	Cl		8.0	110	7.1	181
53		Cl	Cl		8.1	121	7.2	146

^aData are means of duplicate experiments.

exposure of **12** were low, with the majority of the administered oral dose recovered in the feces as the parent molecule. Solubility of **12** in FeSSIF (0.82 mg/mL) was substantially higher than initial hit **15** (0.36 mg/mL), demonstrating the impact of the PSA probe vector added at C-ring R₄. As its physical attributes suggest, **12** had very low measured apparent permeability and an efflux ratio greater than 7 in Madin–Darby Canine Kidney (MDCK) monolayers.

The efficacy of **12** was therefore characterized in a mouse model of obesity and insulin resistance.⁵² To evaluate the PK and PD of **12**, diet-induced obese (DIO) male C57BL/6 mice were fasted and dosed orally with **12** (30 or 100 mg/kg) or vehicle and sacrificed 4, 8, 12, or 16 h postdose. Plasma tGLP-1 and **12** levels were assessed; **12** at both 30 and 100 mg/kg elicited robust and sustained tGLP-1 secretion (Figure 5a) versus vehicle. Again, very low plasma levels of **12** were detected, supportive of a luminal site of action (Figure 5b). The additive influence of sustained incretin exposure on insulin resistance was also assessed in DIO male C57BL/6 mice, dosed orally with vehicle, dipeptidyl peptidase-4 inhibitor sitagliptin, **12** (30 mg/kg), or **12** (30 mg/kg) plus sitagliptin for 85 days. Compound **12** (30 mg/kg) and sitagliptin had a robust additive effect to decrease 6 h fasted plasma insulin levels at day 28 and day 85 (Figure 6).

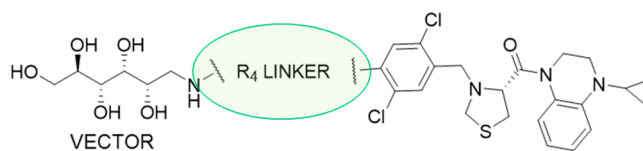
To assess the potential for **12** to inhibit meal-induced gallbladder emptying, as opposed to the gallbladder filling effect we had previously assessed, we used the standard female

CD-1 mouse model.⁵³ Mice (fasted overnight) were dosed orally with **12** (30 mg/kg), systemic TGR5 agonist INT-777 **1** (30 mg/kg), or vehicle, then 1 h 45 min later fed saline or egg yolk. After an additional 15 min, their gallbladders were removed and weighed. Compound **1** was found to strongly inhibit egg yolk-stimulated gallbladder emptying (Figure 7a,b). In contrast, gut-restricted TGR5 agonist **12** did not inhibit gallbladder emptying. In a separate experiment with a similar protocol, **12** at 100 mg/kg again did not inhibit gallbladder emptying (Figure 7c).

DISCUSSION AND CONCLUSIONS

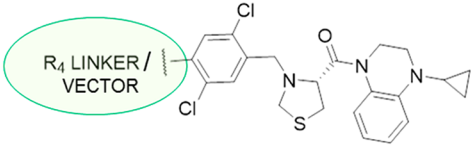
TGR5 is an attractive drug target owing to its modulation of a variety of metabolic, proliferative, and inflammatory pathways. However, TGR5 agonists have historically been associated with undesirable side effects, such as excessive gallbladder filling and blockade of gallbladder emptying, caused by systemic agonism of the receptor in tissues throughout the body. Gut-restricted TGR5 agonists have the potential to avoid these side effects and so be developed into drugs with acceptable safety profiles.

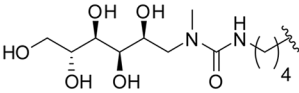
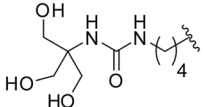
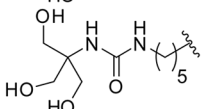
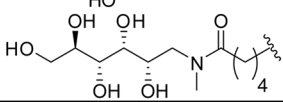
Here, we report the identification and optimization of a series of minimally systemic thiazolidine chemotype TGR5 agonists. Designing a nonaryl structural isostere of a previously disclosed systemic TGR5 agonist chemotype,⁴³ we identified a novel core with improved potency and collected detailed in

Table 5. SAR of PSA Probe/Vector Series (Part 2)⁴²

Compound	R ₄	TGR5 mouse		TGR5 human	
		pEC ₅₀	Efficacy (%)	pEC ₅₀	Efficacy (%)
25	H	7.6	97	7.6	116
50		8.2	106	7.5	174
54		8.5	77	7.4	127
12		8.9	78	6.9	115
55		8.6	74	7.0	124
56		7.8	72	6.6	96
57		8	81	6.7	132
58		7.5	78	6.6	152
59		8.4	112	7.0	132
60		8.1	90	6.7	106
61		8.7	100	7.1	128
62		7.6	107	7.0	96
63		7.5	119	7.0	108
64		8.7	76	7.5	122
65		8.4	100	7.1	161
66		7.9	66	7.0	113

Table 5. continued



Compound	R ₄	TGR5 mouse		TGR5 human	
		pEC ₅₀	Efficacy (%)	pEC ₅₀	Efficacy (%)
67		8.4	82	7.2	152
68		8.0	88	7.0	136
69		9.0	100	7.5	209
70		8.7	72	7.6	176

^aData are means of duplicate experiments.

vitro SAR information in all regions of the new chemotype. We then applied systematic strategies to maximize gut restriction of the novel chemotype, making it minimally systemic, and to optimize PD response in vivo. Our work identified **12**, which has proved to be a useful tool to probe the efficacy of gut-restricted TGR5 agonists. Compound **12** stimulates extended and robust tGLP-1 secretion with negligible systemic compound exposure, supportive of a luminal site of action, with minimal TGR5-mediated suppression of gallbladder emptying.

Our experience with low-exposure molecules and recent publications on beyond-rule-of-five compounds⁵⁴ make it clear that polar compounds of high molecular weight can be surprisingly bioavailable. Limiting permeation by passive and facilitated mechanisms is particularly important for TGR5 agonists as, once systemic, any compound not metabolized to inactive metabolites is largely concentrated in the gallbladder. In this work we define the optimal side chain properties for excluding the thiazolidine chemotype from systemic circulation, gallbladder tissue, and bile, while maintaining target activity locally in the lumen of the intestinal tract (Table 6). The neutral hydrogen bond donating functionality provided by polyols, as opposed to peptidic or charged functionality, provided the most effective presentation of polarity in this regard. In most instances, charged functionality in compounds with comparable mouse TGR5 agonist potency was deleterious to in vivo activity, as in **71**, **72**, **73**, and **77**. This observation demonstrates that engaging targets in the lumen of the gastrointestinal tract is complicated by other factors, and achieving a high local concentration of a potent compound does not equate to a pharmacodynamic response. Compound **74**, a glutamate amide, had moderate PD activity in terms of elevated circulating tGLP-1 but had high activity and concentration in gallbladder relative to other examples with

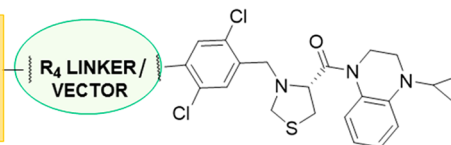
similar properties, suggestive of transport-mediated exposure. Our investigation of the relationship between calculated physical properties and tGLP-1 PD response in vivo revealed that activity is favorable at ~170 Å² PSA and cLogP 1.5–2.2, falling off rapidly above and below these values (Figure 4c,d).

In recent years, other intestine-targeted TGR5 agonists have been identified. These molecules show hypoglycemic activity in mouse models of type 2 diabetes mellitus, with reduced gallbladder-based side effects versus absorbed TGR5 agonists.^{38–40} Compound **5** (Figure 1) discovered by Cao et al.³⁸ has the same A- and C-rings as **12** but has a thiophene B-ring, and it uses a quaternary ammonium-based C-ring vector to increase solubility and minimize compound absorption. Compound **7** (Figure 1) reported by Ma et al.⁴⁰ also shares the same A- and C-rings as **12** and **5** but contains a pyridine B-ring. Its C-ring vector is appended to the DPP-4 inhibitor linagliptin, which has high molecular weight and polarity. In this example, the desirable effect of limiting the deactivation of circulating active GLP-1 by DPP-4 would appear to be contrary with the goal of limiting systemic exposure. Lastly, compound **6** (Figure 1), reported by Duan et al.,³⁹ has the same A-, B-, and C-rings as **7** but is a dimer linked by the C-ring vectors of the two monomers. In each of these examples, systemic effects on the gallbladder were reduced but not eliminated.

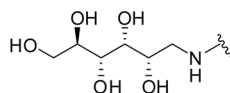
The challenges encountered in designing minimally systemic TGR5 agonists are considerable, not least because of the complex mechanisms by which the gallbladder is controlled. Gallbladder filling and emptying are physiologically distinct, and each function is mediated by both TGR5-dependent and -independent pathways. Filling is mediated by TGR5 in the epithelium of the gallbladder and bile canaliculus by increasing chloride ion transport and thus osmotic water transport into the lumen.³³ Agonism of TGR5 in the smooth muscle tissue of

Table 6. Potency, PD, PK, and Molecular Properties of PSA Probe Thiazolidine Series⁴⁴

PSA probe
Charge
Molecular weight
Hydrogen bonding



PSA probe moiety for
compounds: 12, 54, 59, 61, 64



Compound	R ₄	TGR5 mouse		Fold change over vehicle 8 h after 30 mg/kg PO		Conc. 8 h after 30 mg/kg PO		Molecular descriptors		
		pEC ₅₀	Eff. (%)	Plasma tGLP-1	GB weight	Bile/GB tissue (μM)	Plasma (ng/mL)	PSA (Å ²)	cLogP	MW (g/mol)
50		8.2	106	1.7	1	0.5	0.5	157.0	1.07	683.6
52		8.0	110	2.4	1.3	1.6	0.9	148.3	1.29	697.7
53		8.1	121	1.8	1.1	25.8	1	148.3	1.29	697.7
54		8.5	77	3.8	1.2	0.3	<1	157.0	1.96	711.7
12		8.9	78	4.3 (n=48)	1.7 (n=48)	0.09	<2	166.3	2.21	761.7
59		8.4	112	1.5	1	0.04	0.7	179.2	1.59	762.7
61		8.7	100	2.2	1.4	0.06	0.5	174.9	1.6	781.8
64		8.7	76	4.8 (n=4)	1.8 (n=4)	0.3	0.7	169.1	1.58	726.7
67		8.4	82	1.3	1.2	0.2	<0.5	160.3	1.8	740.7
69		9.0	72	3.5 (n=2)	1.8 (n=2)	6	1.2	148.3	2.18	725.7
70		8.7	100	1.5	2	1.3	3.6	128.6	3.15	680.7
71		8.0	73	1.5	1.6	4.7	ND	104.6	1.72	649.6
72		8.6	92	0.7	0.8	0.08	2.8	119.9	2.67	739.7
73		8.0	73	1.3	1.3	3.1	24.8	125.5	2.78	670.6

Table 6. continued

Compound	R ₄	TGR5 mouse		Fold change over vehicle 8 h after 30 mg/kg PO		Conc. 8 h after 30 mg/kg PO		Molecular descriptors		
		pEC ₅₀	Eff. (%)	Plasma tGLP-1	GB weight	Bile/GB tissue (μM)	Plasma (ng/mL)	PSA (Å ²)	cLogP	MW (g/mol)
74		8.2	64	3	2.5	30.8	2	130.5	3.86	677.6
75		8.4	79	1.9	1.4	1.7	0.6	151.4	3.57	761.8
76		8.7	80	1.6	1.5	0.6	<0.5	151.4	1.72	719.7
77		8.4	98	1.8	1.2	3.9	28.1	174.1	1.47	725.7
78		7.9	86	1.1	1.4	3.7	ND	185.6	0.91	769.7
79		8.0	88	1.4	1.3	1.9	2.3	214.7	0.57	854.8
80		7.4	69	1.2	1.1	0.3	ND	328.9	-3.87	1049.0
81		8.7	67	1.5 (n=2)	1.3 (n=2)	<0.1	<10	377.4	6.22	1673.6

^aTGR5 data are means of duplicate experiments. Unless otherwise stated, other experimental data are the means of data from eight mice.

the gallbladder suppresses contractility, thus inhibiting emptying.⁵⁵ Dramatic distension and retention of bile occurs with concurrent TGR5-induced gallbladder filling and suppression of meal-induced emptying. TGR5 agonist exposure in the lumen of the biliary tract and in the tissues of the gallbladder must therefore both be minimized. Independent of TGR5, circulating active GLP-2 affects the tone of smooth muscle in the wall of the gallbladder, promoting filling.⁵⁶ A low-level filling effect is evident both in our data and the other aforementioned low-exposure TGR5 agonists,^{38–40} which is attributable to increased plasma GLP-2.

In conclusion, through a systematic SAR optimization that included tuning of performance in the gastrointestinal lumen, we identified the gut-restricted thiazolidine TGR5 agonist **12**, which stimulates robust and sustained GLP-1 secretion with minimal TGR5-mediated suppression of gallbladder emptying. Compound **12** is an optimized tool for elucidation of the physiological responses to TGR5 agonist-elicited incretin effects without systemic target engagement. Work is ongoing to evaluate the potential of next generation gut-restricted

TGR5 agonists, building on the performance characteristics of **12**, for the treatment of patients with type 2 diabetes mellitus, NAFLD/NASH, or IBD.

EXPERIMENTAL SECTION

Computational Chemistry. SAR studies identified conserved functionality on a subset of known small-molecule TGR5 agonists. Representative chemotype examples of small-molecule and BA TGR5 agonists, including **8**, **10**, **11**, **13**, and **14**, were used as a data set to generate a pharmacophore alignment model of the conserved functionality. The pharmacophore alignment model was used initially to inform efforts to identify solvent-exposed vectors within favored chemotypes.

The pharmacophore model was generated by identifying lowest energy conformation of key analogs from the series, followed by rigid superposition of those conformers based on volume and feature display. All calculations were performed using the MOE 2009.10 platform (Chemical Computing Group, Montreal, Quebec, Canada). The model was checked for consistency with known SAR by performing flexible alignment of both active and inactive compounds from the remaining data set. The lowest energy ligand conformations were identified using Low Mode MD conformational search,^{57,58} with

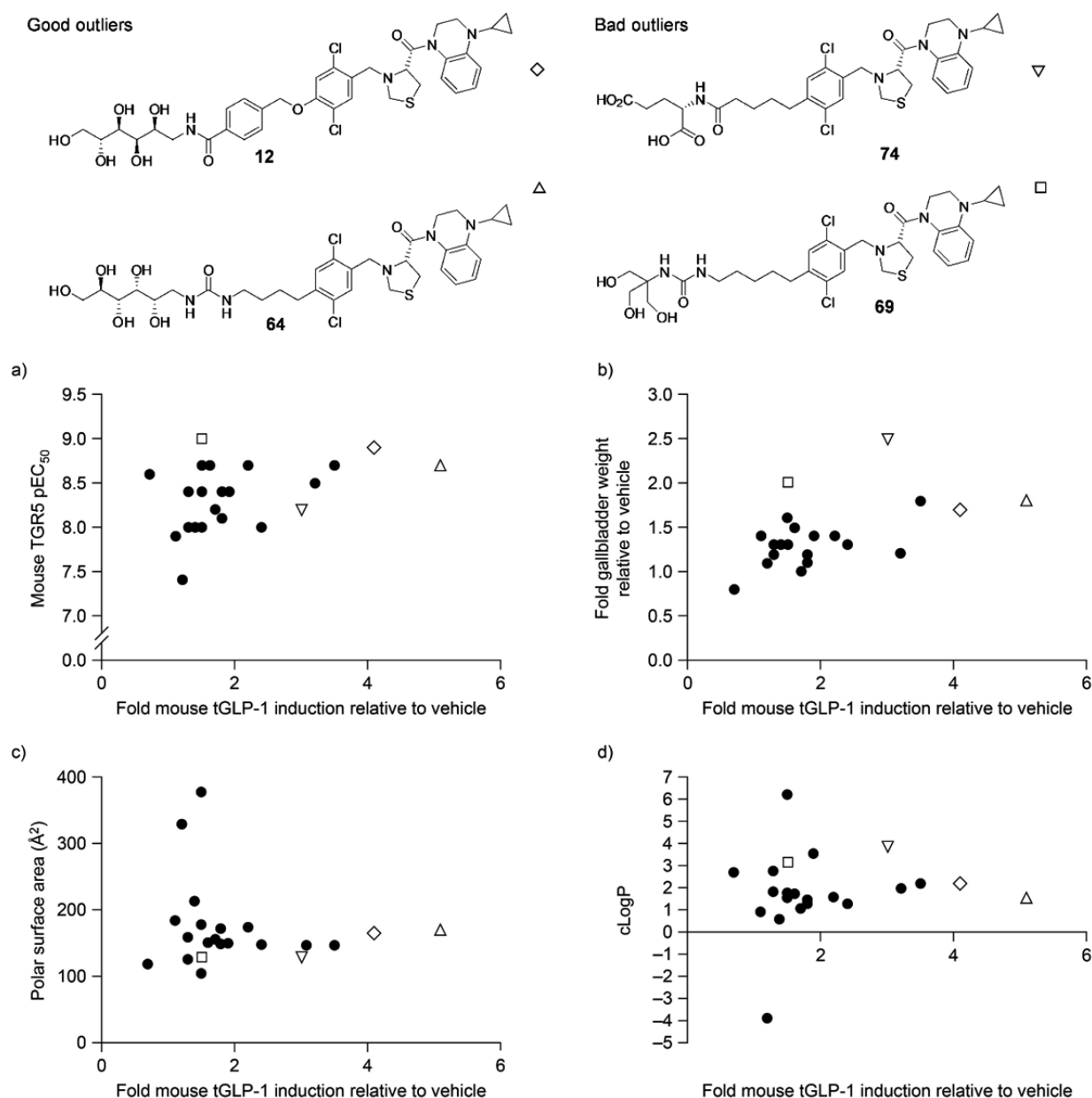


Figure 4. Compound properties and in vivo PK/PD performance of the 22-compound R₄ PSA probe-appended thiazolidine set. Structures of outliers for good and bad performance are shown. Graphs show compound attribute versus fold tGLP-1 induction for (a) in vitro mouse TGR5 pEC₅₀, (b) gallbladder weight in C57BL/6 male mice, (c) PSA, and (d) cLogP.

the MMFF94 force field as implemented in MOE. The flexible alignment algorithm⁵⁹ was used in rigid body mode for key training analogs and in flexible mode for the remainder of the data set.

Observations collected in the course of ongoing SAR studies on select chemotype examples 16 and 17 were used to refine and update the pharmacophore alignment model. Hypotheses on the bioactive conformation adopted by these ligands are supported by the overlay of the global low energy conformers of 15 and 10.

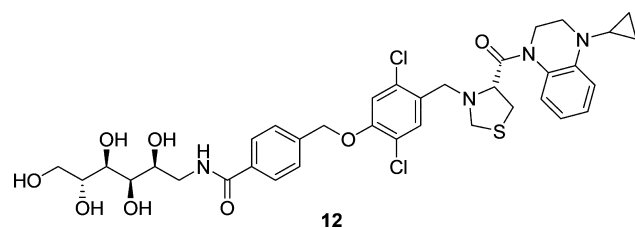
General Chemistry Methods. Unless otherwise stated, reagents and solvents were used as received from commercial suppliers. Proton NMR spectra were obtained with either a Varian spectrometer at 400 MHz or Bruker spectrometer at 300 and 500 MHz. Spectra are given in ppm (δ), and coupling constants, J , are reported in Hertz. TMS ($\delta = 0$) or the solvent peak were used as an internal reference of chemical shift. Unless otherwise specified, purity and low resolution mass spectral data were measured using a Thermo Finnigan Surveyor HPLC system with Surveyor photodiode array detection and a Thermo LCQ Fleet ion trap mass spectrometer, using a Synergi 4 μ m,

hydro-RP80A, 30 \times 2.0 mm column with a flow rate of 0.50 mL/min (solvent A [water + 0.1% formic acid], solvent B [acetonitrile + 0.1% formic acid], gradient: 2% B at $t = 0$ to 95% B at 3 min to 95% B at 3.3 min) or a Shimadzu LC-MS-2020 with SPD-M20A photodiode array detection fitted with a Shim-pack XR-ODS 2.2 μ m, 50 \times 3.0 mm column with a flow rate of 1.0 mL/min (solvent A [water + 0.05% TFA], solvent B [acetonitrile + 0.05% TFA], gradient: 5% B at $t = 0$ to 100% B at 2.0 min to 100% B at 3.2 min). High-resolution quantitative time-of-flight mass spectra were obtained on a Waters Synapt G2-Si instrument.

All tested compounds had a purity of at least 95% as judged by HPLC or LC-MS described above.

Compound Synthesis. Representative synthetic methods are described below. Full synthetic methods for all compounds are provided in [Supporting Information](#).

4-(2,5-Dichloro-4-[[4R]-4-[(4-cyclopropyl-1,2,3,4-tetrahydroquinolin-1-yl)carbonyl]-1,3-thiazolidin-3-yl)methyl]-phenoxy)methyl)-N-[(2S,3R,4R,5R)-2,3,4,5,6-pentahydroxyhexyl]-

Table 7. PK/PD Profile of Optimized TGR5 Agonist **12**

Attribute	Compound 12
human TGR5 EC ₅₀ (nM)	143
mouse TGR5 EC ₅₀ (nM)	1.2
systemic plasma C _{max} (ng/mL) ^a	2 ± 0.3
systemic plasma AUC (ng·h/mL) ^a	<5
fecal recovery (% of dose after 48 h) ^a	83 ± 2.6
gallbladder (plus bile) recovery (% of dose) ^b	<0.01
solubility in FeSSIF pH 6.5 (mg/mL)	0.82
permeability in MDCK monolayers	
P _{app} A → B (cm/s)	<0.01 × 10 ⁻⁶
P _{app} B → A (cm/s)	0.07 × 10 ⁻⁶
efflux ratio, B → A/A → B	>7.0

^aMice dosed orally at 10 mg/kg. ^bMice dosed orally at 30 mg/kg.

benzamide (**12**) (Schemes 3 and 4). Step 1: Synthesis of (4R)-3-[(tert-Butoxy)carbonyl]-1,3-thiazolidine-4-carboxylic Acid **97**. To a solution of (4R)-1,3-thiazolidine-4-carboxylic acid (9 g, 67.6 mmol, 1.00 equiv) in dioxane (100 mL) was added sodium hydroxide (8.1 g, 203 mmol, 3.00 equiv) in water (350 mL) and then (Boc)₂O (22 g, 101 mmol, 1.49 equiv). The resulting solution was stirred overnight at room temperature. The pH value of the solution was adjusted to 4 with hydrogen chloride (1 M) and was then extracted with ethyl

acetate (3 × 250 mL). The combined organic layers were washed with brine (2 × 500 mL), dried over anhydrous sodium sulfate, and concentrated under vacuum to afford 15 g (95%) of **97** as a white solid, which was used without further purification.

Step 2: Synthesis of tert-Butyl (4R)-4-[(4-Cyclopropyl-1,2,3,4-tetrahydroquinoxalin-1-yl)carbonyl]-1,3-thiazolidine-3-carboxylate **98**. A solution of **97** (8.0 g, 34.3 mmol, 1.00 equiv), 1-cyclopropyl-1,2,3,4-tetrahydroquinoxaline (6 g, 34.4 mmol, 1.00 equiv), HATU (17 g, 44.71 mmol, 1.30 equiv), and DIEA (6.7 g, 51.8 mmol, 1.51 equiv) was stirred in DMF (80 mL) overnight. The resulting solution was diluted with H₂O (500 mL) and extracted with ethyl acetate (2 × 250 mL), and the combined organic layers were washed with brine (2 × 500 mL), dried over anhydrous sodium sulfate, and concentrated under vacuum. The residue was purified by silica gel column chromatography with an eluent gradient of petroleum ether/ethyl acetate (20:1 to 10:1) to furnish **98** (12 g, 90%) as a yellow oil.

Step 3: synthesis of 1-Cyclopropyl-4-[[[(4R)-1,3-thiazolidin-4-yl]carbonyl]-1,2,3,4-tetrahydroquinoxaline **99**. To a solution of **98** (10 g, 25.7 mmol, 1.00 equiv) in 1,4-dioxane (150 mL) was added concentrated HCl (50 mL). The resulting solution was stirred for 1 h at room temperature, then the pH value of the solution was adjusted to ~6–7 with aqueous sodium hydroxide, and the resulting solution was extracted with ethyl acetate (2 × 300 mL). The organic layers were combined, washed with brine (3 × 500 mL), dried over anhydrous sodium sulfate, and concentrated under vacuum. The residue was purified by silica gel column chromatography with an eluent gradient of ethyl acetate/petroleum ether (1:10 to 1:4) to furnish **99** (4.98 g, 67%) as a light yellow oil. MS (ES, *m/z*): 290 [M + H]⁺. ¹H NMR (400 MHz, CDCl₃): 7.28–7.11 (m, 3H), 6.74–6.70 (m, 1H), 4.45–4.43 (d, *J* = 9.6 Hz, 1H), 4.14–4.00 (m, 3H), 3.80–3.77 (m, 1H), 3.44–3.41 (t, *J* = 5, 6, 6 Hz, 2H), 2.97–2.93 (t, *J* = 9.6, 6.8 Hz, 1H), 2.74–2.69 (t, *J* = 9.6, 9.2 Hz, 2H), 2.48–2.44 (m, 1H), 0.88–0.84 (m, 2H), 0.69–0.60 (m, 2H).

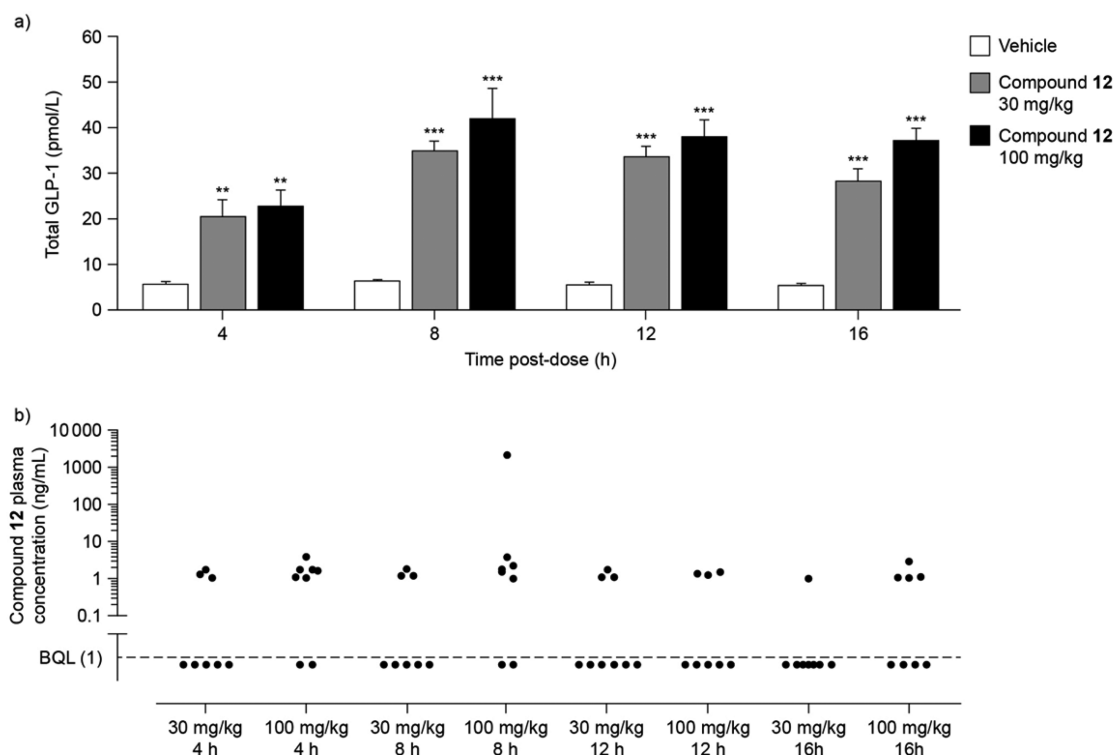


Figure 5. PK and PD of lead compound **12**. (a) Duration of action and (b) extent of plasma exposure of **12** in male C57BL/6 DIO mice. Mice were fasted and sacrificed 4, 8, 12, or 16 h postdosing with **12** 30 or 100 mg/kg, or vehicle (*n* = 8/group except for vehicle 12 h group, *n* = 7). Significance was assessed using two-way ANOVA followed by Bonferroni's posthoc test. ***p* < 0.01; ****p* < 0.001 versus vehicle at the same time point.

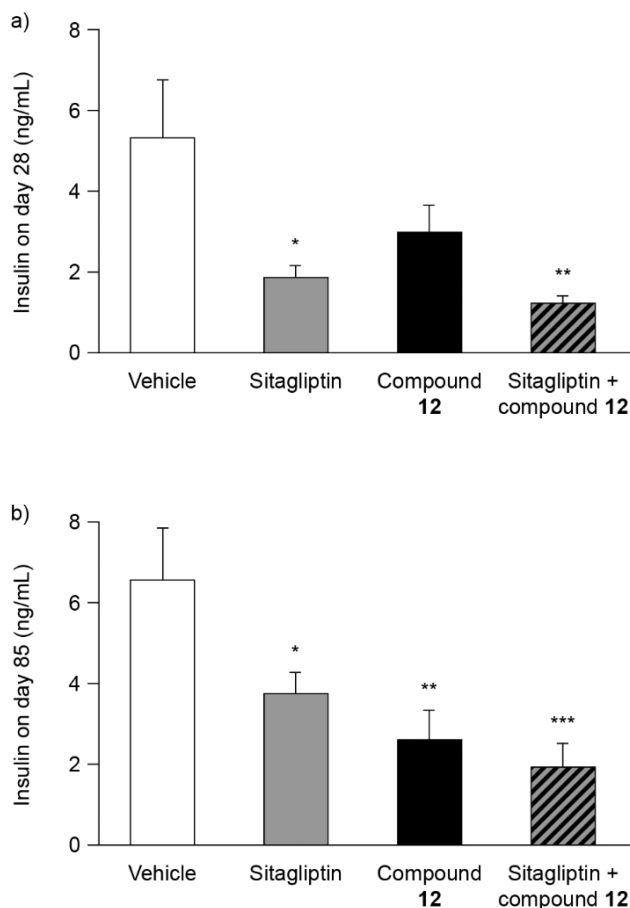


Figure 6. Effect of compound **12** on insulin resistance in a diet-induced obesity mouse model, with and without DPP-4 inhibitor sitagliptin, after (a) 28 days and (b) 85 days of dosing. C57Bl/6 mice ($n = 12/\text{group}$) fed a high fat diet were dosed **12** (30 mg/kg orally) and sitagliptin (0.35% formulated in the diet), daily for 85 days. Mice were then fasted for 5–6 h before sampling of blood for assessment of plasma insulin levels. Significance was assessed using one-way ANOVA with Holm-Sidak's test. * $p < 0.05$; ** $p < 0.01$; *** $p < 0.001$ versus vehicle.

Step 4: Synthesis of 2,5-Dichloro-4-methoxybenzaldehyde 82. To a stirred 0 °C solution of 1,4-dichloro-2-methoxybenzene (25.0 g, 141.2 mmol, 1.00 equiv) and TiCl_4 (30.9 mL) in dichloromethane (300 mL) was added dichloro(methoxy)methane (16.2 g, 140.9 mmol, 1.00 equiv) dropwise. The resulting reaction mixture was stirred for 2 h at 60 °C then quenched by the addition of water/ice. The pH of the solution was adjusted to 1.0 with concentrated HCl extracted with ethyl acetate (4 × 500 mL), and the combined organic layers were washed with brine (2 × 500 mL), dried over anhydrous sodium sulfate, and concentrated under reduced pressure to provide 31.0 g (crude) of **82** as a yellow solid.

Step 5: Synthesis of 2,5-Dichloro-4-hydroxybenzaldehyde 83. A solution of **82** (14.0 g, 68.3 mmol, 1.00 equiv) and LiCl (11.6 g, 274 mmol, 4.00 equiv) in DMF (150 mL) under an inert atmosphere of nitrogen was stirred overnight at 140 °C in an oil bath. The reaction mixture was then quenched by the addition of water/ice, and the pH value of the solution was adjusted to ~1–2 with concentrated HCl. The resulting solution was extracted with ethyl acetate (3 × 400 mL), and the combined organic layers were dried over anhydrous sodium sulfate and concentrated under reduced pressure. The resulting residue was purified using silica gel column chromatography with an ethyl acetate/petroleum ether (1:10–1:5) gradient to provide 10.0 g (77%) of **83** as a light yellow solid. (300 MHz, $\text{DMSO}-d_6$): δ 11.99 (s, 1H), 10.08 (s, 1H), 7.81 (s, 1H), 7.09 (s, 1H).

Step 6: Synthesis of (R)-(4-Cyclopropyl-3,4-dihydroquinoxalin-1(2H)-yl)(3-(2,5-dichloro-4-hydroxybenzyl)thiazolidin-4-yl)-methanone 42. To a solution of **99** (200 mg, 0.691 mmol), **83** (132 mg, 0.691 mmol), and AcOH (40 μL , 0.69 mmol) in DCE (3 mL) was added $\text{NaBH}(\text{OAc})_3$ (234 mg, 1.11 mmol), and the resulting mixture was stirred for 16 h. The excess $\text{NaBH}(\text{OAc})_3$ was quenched with 1 M aqueous HCl, and the mixture was then extracted with DCM. The organic layer was dried over anhydrous sodium sulfate, and the solvent removed under reduced pressure. The resulting residue was purified by flash column chromatography, using a gradient of ethyl acetate in hexanes (9:1–1:1) as eluent resulting in **42** as a white powder (140 mg, 44%). MS (ES, m/z): 464.16 $[\text{M} + \text{H}]^+$. ^1H NMR (400 MHz, CDCl_3) δ 7.62 (bs, 1H), 7.51 (s, 1H), 7.21–7.13 (m, 2H), 7.04 (s, 1H), 6.89 (d, $J = 7.6$ Hz, 1H), 6.76–6.63 (m, 1H), 4.98–4.85 (m, 1H), 4.65 (d, $J = 10.3$ Hz, 1H), 4.54–4.22 (m, 3H), 4.09–3.91 (m, 1H), 3.69–3.53 (m, 1H), 3.46–3.28 (m, 2H), 3.19–2.93 (m, 2H), 2.48–2.35 (m, 1H), 0.91–0.77 (m, 2H), 0.74–0.44 (m, 2H).

Step 7: Synthesis of (R)-4-((2,5-Dichloro-4-((4-(4-cyclopropyl-1,2,3,4-tetrahydroquinoxaline-1-carbonyl)thiazolidin-3-yl)methyl)phenoxy)methyl)benzoic Acid 43. To **42** (172 mg, 0.370 mmol), methyl 4-(hydroxymethyl)benzoate (77 mg, 0.46 mmol), and triphenylphosphine (121 mg, 0.46 mmol) in DCM (3 mL) at 0 °C was added diisopropyl azodicarboxylate (91 μL , 0.46 mmol), and the mixture was allowed to warm to room temperature and then stirred for 16 h. The solvent was removed, and the residue was dissolved in a mixture of H_2O (5 mL) and 1,4-dioxane (25 mL). To this was added $\text{LiOH}\cdot\text{H}_2\text{O}$ (62 mg, 1.5 mmol), and the mixture was stirred at room temperature for 2 h. The solvent was removed, the residue dissolved in DCM and then washed with 1 M aqueous HCl, dried over anhydrous sodium sulfate, and concentrated under reduced pressure, a portion of which was purified by preparative HPLC reverse-phase (C18) to afford **43**. ^1H NMR (400 MHz, CDCl_3) δ 8.12 (d, $J = 8.2$ Hz, 2H), 8.03 (s, 1H), 7.56 (d, $J = 7.9$ Hz, 2H), 7.47 (s, 1H), 7.14 (s, 2H), 6.96–6.82 (m, 2H), 6.65 (s, 1H), 5.18 (s, 2H), 4.87–4.74 (m, 1H), 4.56 (d, $J = 10.2$ Hz, 1H), 4.23 (t, $J = 11.1$ Hz, 2H), 4.11 (d, $J = 13.7$ Hz, 1H), 4.01–3.88 (m, 1H), 3.77–3.60 (m, 1H), 3.46–3.26 (m, 2H), 3.14–3.00 (m, 2H), 2.48–2.31 (m, 1H), 0.89–0.73 (m, 2H), 0.70–0.46 (m, 2H). HRMS-QTOF (m/z): $[\text{M} + \text{H}]^+$ Calcd for $\text{C}_{30}\text{H}_{29}\text{Cl}_2\text{N}_3\text{O}_4\text{S}$, 598.1334; found, 598.1337.

Step 8: Synthesis of 4-(2,5-Dichloro-4-(((4R)-4-[(4-cyclopropyl-1,2,3,4-tetrahydroquinoxalin-1-yl)carbonyl]-1,3-thiazolidin-3-yl)methyl)phenoxy)methyl)-N-[(2S,3R,4R,5R)-2,3,4,5,6-pentahydroxyhexyl]benzamide 12. To a portion of the crude residue of **43** above (~0.123 mmol), D-glucamine (42 mg, 0.23 mmol), and DIEA (128 μL , 0.740 mmol) in DMF (2 mL) was added HATU (70 mg, 0.19 mmol), and the reaction was stirred for 1 h. The mixture was diluted with H_2O , acidified with TFA, and then purified by preparative HPLC with a C18 silica gel stationary phase using a gradient of H_2O 0.05% TFA/ CH_3CN 0.05% TFA (70:30 to 5:95) and detection by UV at 254 nm to give the title compound **12** (21 mg, 17% based on an assumption of 100% purity for **43**) as a bis-trifluoroacetate salt. MS (ES, m/z): 761.34 $[\text{M} + \text{H}]^+$. ^1H NMR (400 MHz, CD_3OD) δ 7.88 (d, $J = 8.0$ Hz, 2H), 7.58 (d, $J = 7.1$ Hz, 2H), 7.25 (s, 1H), 7.20 (dd, $J = 8.3, 1.3$ Hz, 1H), 7.17–7.08 (m, 2H), 7.08–6.99 (m, 1H), 6.67 (t, $J = 7.2$ Hz, 1H), 5.25 (s, 2H), 4.80–4.72 (m, 1H), 4.29 (d, $J = 9.9$ Hz, 1H), 4.14–3.86 (m, 4H), 3.86–3.76 (m, 3H), 3.76–3.61 (m, 5H), 3.61–3.51 (m, 1H), 3.47 (dd, $J = 13.7, 7.3$ Hz, 1H), 3.43–3.35 (m, 1H), 3.21–3.09 (m, 2H), 2.44 (s, 1H), 0.80 (s, 2H), 0.56 (s, 2H). HRMS-QTOF (m/z): $[\text{M} + \text{H}]^+$ Calculated for $\text{C}_{36}\text{H}_{43}\text{Cl}_2\text{N}_4\text{O}_8\text{S}$, 761.2178; found, 761.2167.

Biology. Cell-Based TGR5 Agonism Assay. Primary cell-based screens were performed in HEK293 cells stably transfected to heterologously express human or mouse TGR5. Cells were treated with candidate TGR5 agonists and assessed for increased intracellular levels of cAMP.

HEK293 cells were transfected with a vector that expresses a gene encoding TGR5, and a stable cell line was isolated using drug selection following standard techniques. The gene encoding human TGR5 (NM_001077191.1 in pCMV6-AC) was obtained from

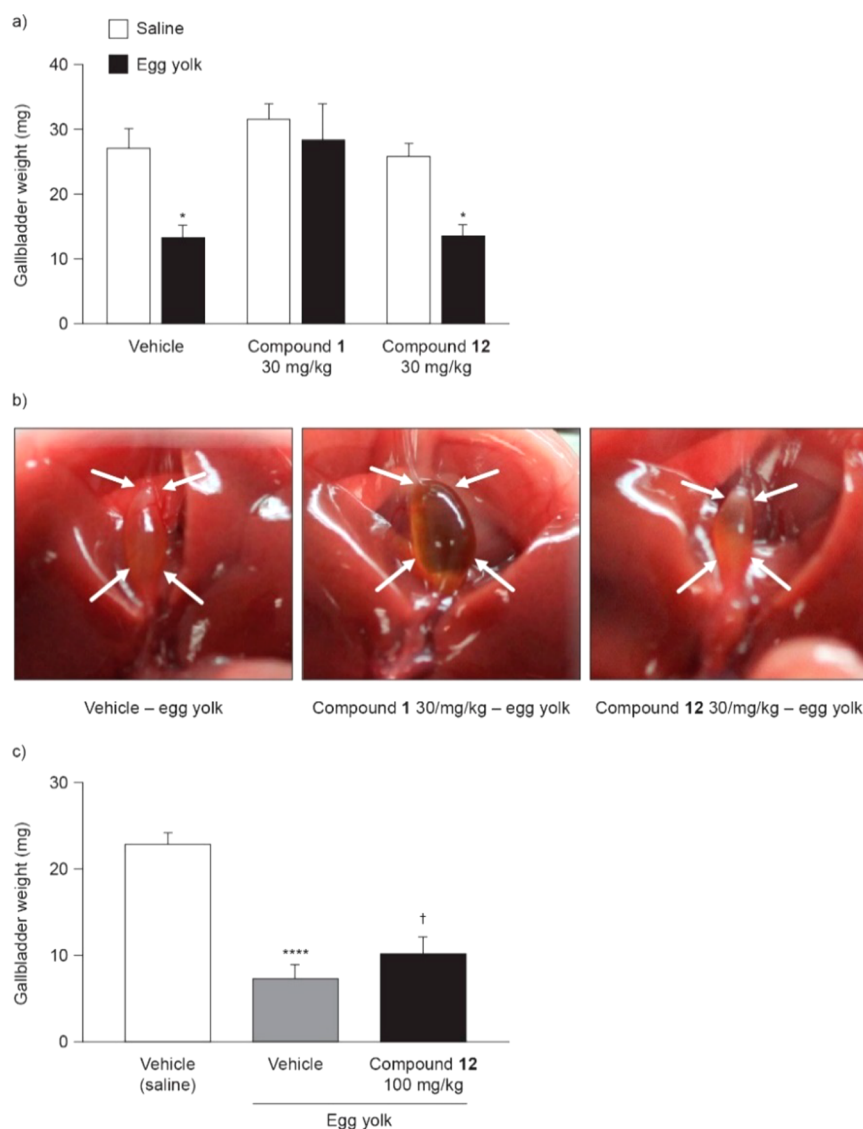


Figure 7. Effect of compound 12 on gallbladder emptying. (a,b) CD-1 female mice ($n = 6/\text{group}$; fasted overnight) were dosed orally with 12 at 30 mg/kg, systemic TGR5 agonist 1 at 30 mg/kg, or vehicle, then challenged orally 1 h 45 min later with saline or egg yolk. After another 15 min, gallbladders were removed and weighed. (a) Gallbladder weight and (b) images of representative gallbladders from egg-yolk-challenged mice are shown. Significance was assessed using two-way ANOVA followed by Bonferroni's posthoc test. $*p < 0.05$ versus saline for each agent dosed. (c) Effect of 12 at 100 mg/kg on gallbladder emptying, evaluated in a separate experiment with a similar protocol. Significance was assessed using one-way ANOVA with Holm-Sidak's test. $****p < 0.0001$ for vehicle (egg yolk) versus vehicle (saline). $†$ No significant difference for 12 100 mg/kg (egg yolk) versus vehicle (egg yolk).

Origene, and a codon-optimized synthetic gene encoding mouse TGR5 (NM_174985.1 in pJ603) was obtained from Atum (Fremont, CA). Cells were grown overnight at 37 °C/5% CO₂ prior to assay.

TGR5-mediated cAMP generation was measured using a homogeneous time-resolved fluorescence (HTRF) detection method (Cisbio, Codolet, France). Test compounds were dissolved in DMSO to a final concentration of 10 nM. Serial 3-fold dilutions of the stock solution were made in DMSO, and these solutions were diluted 100-fold into HBSS supplemented with 10 mM HEPES pH 7.4 and 0.5 mM IBMX. Prior to assay, culture medium was replaced with fresh medium, and test compounds diluted in HBSS/HEPES/IBMX were added to the cells and incubated at 37 °C for 30 min. Each compound was tested in duplicate at 12 concentrations ranging from 0.05 nM to 10 μM.

Following incubation with test compounds, cAMP was detected through the successive addition of cAMP labeled with the modified allophycocyanin dye d2 (cAMP-d2) and cryptate-labeled anti-cAMP in lysis buffer and reading HTRF per the instructions provided by the

manufacturer Cisbio. A standard curve was used to convert the raw HTRF data into [cAMP], which was plotted against log[test compound], and the resulting curves were fitted to a 3-parameter logistical equation using GraphPad Prism to determine pEC₅₀ (the negative log of the EC₅₀) and the magnitude of the response. The magnitude of the maximum response (% efficacy) was typically between 50 and 200% of the maximum response elicited by a benchmark compound 11⁴⁴ (Figure 1), which had a maximum response similar to that elicited by lithocholic acid 13 (Figure 2).

Determination of Compound Solubility in Fed State Simulated Intestinal Fluid (FeSSIF). A total of 200 μL of test compound (1 mg/mL in DCM) was dispensed into glass inserts in a 96-well plate and dried overnight. SIF powder (Biorelevant.com, London, UK) was dissolved to 11.2 mg/mL in pH 6.5 buffer to prepare FeSSIF. Samples were dissolved in an equivalent volume of FeSSIF pH 6.5 to produce test compound samples with a nominal concentration of 1 mg/mL. Quality control samples were included in the same plate and prepared by drying 20 or 160 μL of test compound (1 mg/mL in DCM)

overnight and dissolving the samples in 200 μL of DMSO to give nominal test compound concentrations of 0.1 and 0.8 mg/mL, respectively. The test and quality control (QC) samples were shaken overnight on an orbital shaker at 625 r.p.m. and filtered through an AcroPrep 0.2 μm GHP (hydrophilic polypropylene) membrane (Pall Corporation, Port Washington, New York, USA). The filtered samples and calibration standards were diluted 1:5 in 50:50 acetonitrile/water in a 96-well HPLC injection plate, and 10 μL of each was injected on an Agilent 1100 series HPLC with a UV detector (Agilent, Santa Clara, CA, USA). Chromatographic separation was performed with a gradient method (A: 0.1% TFA; B: acetonitrile) on a Zorbax SB-Phenyl 150 \times 4.6 mm, 5 μm particle analytical column (Agilent). The flow rate was 1 mL/min with the following gradient: 10–95% B for 7 min, 95% B for 1 min, and column equilibration with 10% B for 1 min. The column eluent was monitored at 230 nm. Test compound concentrations were interpolated from a linear equation of a calibration curve based on the peak areas calculated at an absorbance of 230 nm using OpenLAB ChemStation software (Agilent).

Animal Ethics. All animal experiments were in accordance with the guidelines as defined by Institutional Animal Care and Use Committee for U.S. institutions.

In Vivo GLP-1 Secretion and Gallbladder Measurement (Single Time Point). C57BL/6 male mice on regular chow had food removed in the morning and were dosed with vehicle ($n = 8$) (10% hydroxypropyl- β -cyclodextrin in 10 mM phosphate-buffered saline or 2% DMSO in 0.4% hydroxypropyl methylcellulose) or test compound ($n = 8$ /compound) in vehicle to achieve a dose of 30 mg/kg. Eight hours later, each mouse was heavily anesthetized with isoflurane, and the peritoneal cavity was opened and the gallbladder, with its entire contents, was carefully excised and weighed. Blood was collected from the left ventricle of the heart and processed to plasma in K₂EDTA-coated tubes for measurement of total GLP-1 using a K150JVC (version 2 total GLP-1) assay kit (Meso Scale Discovery, Gaithersburg, MD, USA).

Determination of Compound Concentration and Dose Recovery in Bile/Gallbladder Tissue. Whole gallbladders were homogenized in 100 μL of water using a polypropylene micropestle. The homogenates were diluted 1:5 with water. To prepare the calibration standards, working solutions of compound prepared in 50:50 acetonitrile/water were diluted 1:10 in a pooled, homogenized gallbladder matrix prepared from animals dosed with vehicle. The compound was extracted with three volumes of acetonitrile containing an internal standard (10 ng/mL labetalol). The extracted samples were centrifuged and the supernatants were diluted 1:3 with 50:50 acetonitrile/water prior to injection on a LC–MS/MS system consisting of a 1260 Infinity HPLC and 6410 triple quadrupole mass spectrometer controlled by MassHunter Acquisition software (Agilent). Chromatographic separation was performed using a Phenomenex Hydro-RP C18 30 \times 2 mm, 4 μm analytical column (Phenomenex, Torrance, CA, USA) with a gradient elution method. Mobile phase A consisted of 0.1% formic acid in water, and mobile phase B consisted of 0.1% formic acid in acetonitrile. The initial flow rate was 0.4 mL/min, and the gradient was as follows: 0–0.3 min at 10% B, 0.3–2.5 min at 10–95% B at 0.6 mL/min flow rate, 2.5–3.5 min at 95% B at 0.6 mL/min flow rate, and 1 min at the initial conditions for column equilibration. Compound concentrations in the study samples were interpolated from a calibration curve based on the peak area ratio of analyte to internal standard and the theoretical concentration of each standard using MassHunter Quantitative Analysis software (Agilent). The analyte and internal standard were ionized using electrospray in positive ionization mode (ESI+). The percentage dose recovery calculations were performed in Microsoft Excel.

Determination of Compound Concentration in Plasma. Blood samples, collected as described in *In Vivo GLP-1 Secretion and Gallbladder Measurement (Single Time Point)*, were processed to plasma by centrifugation for PK analysis. The compound was quantified in plasma samples by LC–MS/MS. Working solutions of the calibration standards and QC samples were prepared in 50:50

acetonitrile/water from a freshly prepared 1 mg/mL stock solution of compound prepared in 50:50 DMSO/acetonitrile. Working solutions of standards were diluted 1:10 in pooled C57BL/6 K₂EDTA plasma (BioreclamationIVT, Liverpool, NY, USA). The QC samples were prepared independently of the standards and assayed throughout the analytical run to confirm quantitation accuracy and precision. Blank plasma samples were also extracted to evaluate selectivity of the method in the plasma matrix. The study samples, standards, and QC samples were extracted with three volumes of acetonitrile containing an internal standard (10 ng/mL labetalol). Precipitated proteins were removed by centrifugation. The supernatants were transferred and diluted with an equal volume of water in a 96-well polypropylene plate for injection with a CTC autosampler connected to a 1260 Infinity HPLC and 6410 triple quadrupole mass spectrometer controlled by MassHunter Acquisition software (Agilent). Chromatographic separation was performed using a Phenomenex Hydro-RP C18 30 \times 2 mm, 4 μm analytical column with a gradient elution method. Mobile phase A consisted of 0.1% formic acid in water and mobile phase B consisted of 0.1% formic acid in acetonitrile. The initial flow rate was 0.4 mL/min, and the gradient was as follows: 0–0.3 min at 10% B, 0.3–2.5 min at 10–95% B at 0.6 mL/min flow rate, 2.5–3.5 min at 95% B at 0.6 mL/min flow rate, and 1 min at the initial conditions for column equilibration. The analyte and internal standard were ionized using electrospray in ESI+ mode. Pharmacokinetic parameter calculations in plasma were performed in Microsoft Excel. The area under the plasma compound concentration–time curve (AUC) was determined using the linear trapezoidal method.

In Vitro Target Selectivity Assays. The effect of the TGR5 agonists on IBAT was assessed using HEK293 cells transfected with a vector that expresses a gene encoding human or mouse IBAT, with inhibition of the uptake of [taurine-³H]taurocholic acid measured in a manner similar to that described by Craddock.⁵¹ IBAT-transfected cells were overlaid with uptake buffer (10 mM HEPES, 116 mM sodium chloride, 5.3 mM KCl, 1.8 mM CaCl₂, 11 mM glucose, 1.1 mM KH₂PO₄, pH 7.4) containing 10 μM [³H]taurocholic acid (American Radiolabeled Chemicals, St. Louis, MO, USA) and 0–26 μM test compound. Following a 40 min incubation, the solution was removed, and the cells were washed twice with uptake buffer. Cells were lysed by addition of 20 μL of 0.1% Tween 80 followed by 100 μL of scintillation fluid and counted using a TopCount (PerkinElmer, Waltham, MA, USA). The assay was benchmarked using taurocholate, deoxycholate, and chenodeoxycholic acid, which each inhibited uptake of [³H]taurocholic acid with potency similar to that reported by Craddock.⁵¹

The potential for the TGR5 agonists to activate FXR (NR1H4) was measured using a cell-based assay kit from Indigo Biosciences (State College, PA, USA). Cells expressing human FXR and a FXR-responsive luciferase reporter gene were grown in duplicate in the presence of 0.4–50 μM test compound in buffer according to the manufacturer's instructions. The assay was benchmarked using GW4064 and chenodeoxycholic acid, which had pEC₅₀ values of 6.8 and 4.0–4.5, respectively, similar to literature reports.⁵⁰

The binding selectivity of the TGR5 agonists against a range of other receptors, transporters, and ion channels was evaluated using an 80-target pharmacology assay panel (Eurofins Cerep Panlabs, St. Charles, MO, USA).

Determination of Fecal Recovery of 12. Fecal samples (48 h collection) were lyophilized and mechanically homogenized to a fine powder. Levels of 12 in feces were quantified using a LC–MS/MS method. Duplicate 25–35 mg aliquots of homogenized fecal samples were prepared. Working solutions of calibration standards and QC samples were prepared in 50:50 acetonitrile/water from a freshly prepared 1 mg/mL stock solution of 12. Working solutions of calibration standards or QCs were added to pooled blank feces (feces from animals dosed with vehicle only). The study samples, standards, and QC samples were extracted with three volumes of acetonitrile containing an internal standard (10 ng/mL labetalol). Samples were vortexed for 10 min and centrifuged for 10 min at 20 000 \times g at room temperature. Supernatants were transferred and diluted 1:4 with water in a 96-well polypropylene plate for injection. The LC–MS/MS

method used was the same as the one used for the plasma PK samples. The percentage dose recovery calculations were performed in Microsoft Excel.

Estimation of Membrane Permeability of 12. Membrane permeability of **12** was estimated using a MDCK bidirectional permeability assay. MDCK cells were cultured into monolayers on 96-well HTS Transwell 24-well 0.4 μm polyester membrane inserts (Corning, NY, USA) for 48 h. On the day of assay, the cell monolayers were washed with transport buffer (HBSS–HEPES pH 7.4). Compound **12** (10 μM in transport buffer with a final DMSO concentration of 0.1%) was added to the donor side of the inserts (on either the apical [A] or basolateral [B] side of the cells) in duplicate, and transport buffer was added to the receiver side. Colchicine (P-glycoprotein [P-gp] substrate with low A to B permeability), labetalol (medium to high permeability), propranolol (high permeability), atenolol (low permeability), and/or ranitidine (low permeability) were assessed separately as controls for each assay. Inserts were incubated at 37 °C for 1 h to allow transport from the A to the B side, or 40 min to allow transport from the B to the A side. The P-gp inhibitor, verapamil, was included on the A and B sides at 100 μM with **12** or control compounds to determine whether **12** was potentially a P-gp substrate. Samples were taken from the donor side before incubation and the donor and receiver sides after incubation, and they were analyzed by HPLC–tandem mass spectrometry (HPLC–MS/MS).

The donor samples were diluted 1:10 with transport buffer. Two volumes of acetonitrile containing labetalol as the internal standard (IS) were added to the donor and receiver samples, vortexed, and centrifuged at 3400 \times g for 10 min at room temperature. Supernatants were transferred and diluted with an equal volume of water in a 96-well polypropylene plate (VWR) for injection with a 1260 Infinity II Multisampler (Agilent) connected to a 1260 HPLC and 6410 triple quadrupole mass spectrometer controlled by MassHunter Acquisition software (Agilent). Chromatographic separation was performed using a Gemini NX-C18 analytical column (30 mm \times 2 mm ID, 5 μm particle; Phenomenex) with a gradient elution method. Mobile phase A consisted of 0.1% formic acid/water. Mobile phase B consisted of 0.1% formic acid/acetonitrile. The analyte and IS were ionized using electrospray in ESI+ mode.

The following equations were used to calculate the P_{app} , efflux ratio (ER), and recovery of **12** in Microsoft Excel. An efflux ratio >2 indicate that they may be potential substrates of one or more efflux transporters. Compound **12** concentration in study samples was interpolated from a standard curve based on the ratio of the peak area of **12** for each calibration sample to the peak area of the IS at each calibration level using MassHunter Quantitative Analysis software (Agilent).

$$P_{\text{app}} = (V_{\text{R}} C_{\text{R, end}}) / (A t C_{\text{D0}})$$

$$ER = (P_{\text{app}} \text{ B to A}) / (P_{\text{app}} \text{ A to B})$$

$$\text{recovery} = [(C_{\text{D, end}} V_{\text{D}}) + (C_{\text{R, end}} V_{\text{R}})] / (C_{\text{D0}} V_{\text{D}}) \times 100$$

where P_{app} is apparent permeability (cm/s); ER is efflux ratio (no units); recovery is assay recovery of compound (%); V_{D} is volume of donor (mL); V_{R} is volume of receiver (mL); C_{D0} is concentration of test compound on donor side at time zero (μM); $C_{\text{D, end}}$ is concentration of test compound on donor side at the end time point (μM); $C_{\text{R, end}}$ is concentration of test compound on receiver side at the end time point (μM); A is surface area of Transwell membrane insert (cm^2); t is total incubation time (s).

Duration of 12 Effect on GLP-Secretion, and 12 Concentration in Plasma. Sets of DIO male C57BL/6 mice (Taconic Biosciences, Germantown, NY, USA) fed Research Diets D12492 (New Brunswick, NJ, USA) for 6.4–7.4 weeks were dosed orally with **12**, 30 or 100 mg/kg, or vehicle (10% hydroxy- β -cyclodextrin in 10 mM phosphate-buffered saline), and groups of mice from each set were sacrificed 4, 8, 12, or 16 h postdose ($n = 8/\text{treatment}$ for each time point). For these time points, mice were fasted for 7, 8, 12, and 16 h, respectively. Mice were heavily anesthetized with isoflurane, and

blood was collected from the left ventricle of the heart and processed to plasma in K_2EDTA -coated tubes. One plasma sample was used for measurement of tGLP-1 using a K150FCC assay kit (Meso Scale Discovery). Another plasma sample was used for measurement of compound concentration by LC–MS/MS using the same method described above for the plasma PK samples. The multiple reaction monitoring transitions used to detect **12** were 761.2 > 298.2 m/z (quantifier) and 761.2 > 135.1 m/z (qualifier).

Determination of 12 Effect on Insulin Resistance. DIO age-matched male C57BL/6 mice (17–18 weeks old; Taconic Biosciences) fed a high-fat diet (D12492, Research Diets) starting at 6 weeks of age were used. Body weight was measured in the fed state, and then the mice were fasted for 5–6 h prior to blood draw. The tip of the tail was removed, and a glucometer reading was taken. Then, $\sim 125 \mu\text{L}$ of blood was milked from the tail into an EDTA-coated microvette tube (#16.444.100; Sarstedt, Newton, NC, USA) and processed to plasma for measurement of insulin levels using a rat/mouse insulin assay kit (Meso Scale Discovery, catalog# K152BZC-2) at baseline. Blood samples were also taken for measurement of insulin levels on day 28 and day 85 using the same procedure. DIO mice were assigned to groups ($n = 12$) such that groups had comparable mean glucose, insulin, and body weight values at baseline. Mice were dosed orally (5 mL/kg), once daily in the afternoon (2:00 p.m.). Dosing groups were vehicle (10% hydroxypropyl- β -cyclodextrin in phosphate-buffered saline), vehicle and sitagliptin 0.35% in food, 30 mg/kg compound **12** in vehicle, and 30 mg/kg compound **12** in vehicle and sitagliptin 0.35% in food. Mice were weighed at 7–11-day intervals. Compounds were formulated weekly, and body weight was used to adjust dosing volume.

In Vivo Measurement of Gallbladder Emptying. CD-1 female mice (Charles River Laboratories, Wilmington, MA, USA) fed regular chow (#2018, Harlan Teklad) had food removed (to prevent gallbladder emptying) in the late evening. The next morning (~ 16 h later), sets of mice ($n = 12/\text{group}$) were dosed orally with vehicle (10% hydroxypropyl- β -cyclodextrin), compound **1** (30 mg/kg), or **12** (30 mg/kg). After 1 h 45 min, half of the mice in each dose set were dosed orally with saline (0.75 mL), and the other half of the mice of each dose set were dosed orally with lyophilized egg yolk (0.75 mL; 30 wt %/vol reconstituted in saline for induction of cholecystokinin-mediated gallbladder emptying). After an additional 15 min, mice were heavily anesthetized with isoflurane, the peritoneal cavity was opened and gallbladders (with contents) were carefully excised and weighed.

In a separate experiment with a similar protocol, one group of six mice was dosed orally with **12** (100 mg/kg) and two groups of six mice were dosed orally with vehicle. After 8 h, one vehicle group was dosed orally with saline, and the **12** group and one vehicle group were dosed orally with egg yolk. Gallbladders were collected and weighed as above.

■ ASSOCIATED CONTENT

📄 Supporting Information

The Supporting Information is available free of charge on the ACS Publications website at DOI: 10.1021/acs.jmedchem.8b00308.

Full synthetic methods and characterization data for compounds **15–81**. CEREP pharmacology panel data for compound **12** (PDF)

Modeling coordinates for Figure 2b (alignment of TGR5 agonist chemotype examples) and Figure 3c (alignment of **10** and **15** low energy conformers) (ZIP)

Molecular formula strings for compounds **1–81** (CSV)

■ AUTHOR INFORMATION

Corresponding Author

*Phone: +1 510 745 1707. E-mail: jlewis@ardelyx.com.

ORCID 

Jason Gustaf Lewis: 0000-0002-1419-653X

Present Addresses

[†](A.G.S.) Millendo Therapeutics, 301 N. Main Street, Suite 100, Ann Arbor, Michigan 48104, United States.[‡](M.N.) Wemberly Scientific, Inc., 1025 Alameda de las Pulgas, #116, Belmont, California 94002, United States.

Notes

The authors declare the following competing financial interest(s): A.G.S., C.W.C., D.C., D.R., M.N., N.B., N.W.R., and P.D.F. are former employees of and retain ownership interest in Ardelyx. All other authors are current employees of and have ownership interest in Ardelyx.

ACKNOWLEDGMENTS

This work was funded by Ardelyx. The authors would like to acknowledge Tony Chen, Ph.D., and Junping Zhang, Ph.D., of Pharmaron LLC for insightful leadership of the synthetic chemistry team contributing compounds to this effort. Pharmacophore alignment was performed by Erin K. Bradley, Ph.D., of LigDCipher. Medical writing support was provided by Richard Claes, Ph.D., and Steven Inglis, Ph.D., of Oxford PharmaGenesis, funded by Ardelyx.

ABBREVIATIONS USED

ANOVA, analysis of variance; AUC, area under the plasma concentration time curve; BA, bile acid; BQL, below quantification limit; cAMP, cyclic adenosine monophosphate; CDI, carbonyldiimidazole; clogP, calculated logarithm of the partition coefficient between *n*-octanol and water; C_{max} , maximum observed plasma concentration; DCE, 1,2-dichloroethane; DCM, dichloromethane; DIAD, diisopropyl-diazo-1,2-dicarboxylate; DIEA, *N,N*-diisopropylethylamine; DIO, diet-induced obese; DMF, dimethylformamide; DMSO, dimethyl sulfoxide; DPP-4, dipeptidylpeptidase-4; EC_{50} , half maximal effective concentration; EDTA, ethylenediaminetetraacetic acid; FeSSIF, fed state simulated intestinal fluid; FXR, farnesoid X receptor; GB, gallbladder; GLP, glucagon-like peptide; GPBAR1, G protein-coupled bile acid receptor 1; HATU, 1-[bis(dimethylamino)methylene]-1*H*-1,2,3-triazolo-[4,5-*b*]pyridinium 3-oxid hexafluorophosphate; HBSS, Hank's Balanced Salt Solution; HEPES, 4-(2-hydroxyethyl)-1-piperazineethanesulfonic acid; HPLC, high-performance liquid chromatography; HTRF, homogeneous time-resolved fluorescence; IBAT, ileal bile acid transporter; IBD, inflammatory bowel disease; IBMX, isobutyl methylxanthine; LC-MS, liquid chromatography-mass spectrometry; LCA, lithocholic acid; MDCK, Madin-Darby Canine Kidney; MW, molecular weight; NAFLD, nonalcoholic fatty liver disease; NASH, nonalcoholic steatohepatitis; ND, not determined; NMR, nuclear magnetic resonance; P_{app} , apparent permeability; PD, pharmacodynamic; pEC_{50} , negative logarithm of the half maximal effective concentration; PK, pharmacokinetic; pK_a , negative base-10 logarithm of the acid dissociation constant; PSA, polar surface area; QTOF, quantitative time-of-flight; SAR, structure-activity relationship; TFA, trifluoroacetic acid; tGLP-1, total glucagon-like peptide 1; TGR5, Takeda G protein-coupled receptor 5; TLCA, tauro-lithocholic acid.

REFERENCES

(1) Li, T.; Chiang, J. Y. Bile acid signaling in metabolic disease and drug therapy. *Pharmacol. Rev.* **2014**, *66*, 948–983.

(2) Kawamata, Y.; Fujii, R.; Hosoya, M.; Harada, M.; Yoshida, H.; Miwa, M.; Fukusumi, S.; Habata, Y.; Itoh, T.; Shintani, Y.; Hinuma, S.; Fujisawa, Y.; Fujino, M. A G protein-coupled receptor responsive to bile acids. *J. Biol. Chem.* **2003**, *278*, 9435–9440.

(3) Maruyama, T.; Miyamoto, Y.; Nakamura, T.; Tamai, Y.; Okada, H.; Sugiyama, E.; Nakamura, T.; Itadani, H.; Tanaka, K. Identification of membrane-type receptor for bile acids (M-BAR). *Biochem. Biophys. Res. Commun.* **2002**, *298*, 714–719.

(4) Duboc, H.; Tache, Y.; Hofmann, A. F. The bile acid TGR5 membrane receptor: from basic research to clinical application. *Dig. Liver Dis.* **2014**, *46*, 302–312.

(5) Ullmer, C.; Alvarez Sanchez, R.; Sprecher, U.; Raab, S.; Mattei, P.; Dehmlow, H.; Sewing, S.; Iglesias, A.; Beauchamp, J.; Conde-Knape, K. Systemic bile acid sensing by G protein-coupled bile acid receptor 1 (GPBAR1) promotes PYY and GLP-1 release. *Br. J. Pharmacol.* **2013**, *169*, 671–684.

(6) Baggio, L. L.; Drucker, D. J. Biology of incretins: GLP-1 and GIP. *Gastroenterology* **2007**, *132*, 2131–2157.

(7) Campbell, J. E.; Drucker, D. J. Pharmacology, physiology, and mechanisms of incretin hormone action. *Cell Metab.* **2013**, *17*, 819–837.

(8) Rowland, K. J.; Brubaker, P. L. The “cryptic” mechanism of action of glucagon-like peptide-2. *Am. J. Physiol Gastrointest Liver Physiol* **2011**, *301*, G1–8.

(9) Davidson, M. B.; Bate, G.; Kirkpatrick, P. Exenatide. *Nat. Rev. Drug Discovery* **2005**, *4*, 713–714.

(10) Drucker, D. J.; Dritselis, A.; Kirkpatrick, P. Liraglutide. *Nat. Rev. Drug Discovery* **2010**, *9*, 267–268.

(11) Hashimoto, E.; Taniai, M.; Tokushige, K. Characteristics and diagnosis of NAFLD/NASH. *J. Gastroenterol. Hepatol.* **2013**, *28* (Suppl 4), 64–70.

(12) Musso, G.; Cassader, M.; De Micheli, F.; Rosina, F.; Orlandi, F.; Gambino, R. Nonalcoholic steatohepatitis versus steatosis: adipose tissue insulin resistance and dysfunctional response to fat ingestion predict liver injury and altered glucose and lipoprotein metabolism. *Hepatology* **2012**, *56*, 933–942.

(13) Lambert, J. E.; Ramos-Roman, M. A.; Browning, J. D.; Parks, E. J. Increased de novo lipogenesis is a distinct characteristic of individuals with nonalcoholic fatty liver disease. *Gastroenterology* **2014**, *146*, 726–735.

(14) Birkenfeld, A. L.; Shulman, G. I. Nonalcoholic fatty liver disease, hepatic insulin resistance, and type 2 diabetes. *Hepatology* **2014**, *59*, 713–723.

(15) Ding, X.; Saxena, N. K.; Lin, S.; Gupta, N. A.; Anania, F. A. Exendin-4, a glucagon-like protein-1 (GLP-1) receptor agonist, reverses hepatic steatosis in ob/ob mice. *Hepatology* **2006**, *43*, 173–181.

(16) Trevasnik, J. L.; Griffin, P. S.; Wittmer, C.; Neuschwander-Tetri, B. A.; Brunt, E. M.; Dolman, C. S.; Erickson, M. R.; Napora, J.; Parkes, D. G.; Roth, J. D. Glucagon-like peptide-1 receptor agonism improves metabolic, biochemical, and histopathological indices of nonalcoholic steatohepatitis in mice. *Am. J. Physiol Gastrointest Liver Physiol* **2012**, *302*, G762–772.

(17) Mells, J. E.; Fu, P. P.; Sharma, S.; Olson, D.; Cheng, L.; Handy, J. A.; Saxena, N. K.; Sorescu, D.; Anania, F. A. Glp-1 analog, liraglutide, ameliorates hepatic steatosis and cardiac hypertrophy in C57BL/6J mice fed a Western diet. *Am. J. Physiol Gastrointest Liver Physiol* **2012**, *302*, G225–235.

(18) Lee, Y. S.; Shin, S.; Shigihara, T.; Hahm, E.; Liu, M. J.; Han, J.; Yoon, J. W.; Jun, H. S. Glucagon-like peptide-1 gene therapy in obese diabetic mice results in long-term cure of diabetes by improving insulin sensitivity and reducing hepatic gluconeogenesis. *Diabetes* **2007**, *56*, 1671–1679.

(19) Armstrong, M. J.; Gaunt, P.; Aithal, G. P.; Barton, D.; Hull, D.; Parker, R.; Hazlehurst, J. M.; Guo, K.; Abouda, G.; Aldersley, M. A.; Stocken, D.; Gough, S. C.; Tomlinson, J. W.; Brown, R. M.; Hubscher, S. G.; Newsome, P. N. Liraglutide safety and efficacy in patients with non-alcoholic steatohepatitis (LEAN): a multicentre,

double-blind, randomised, placebo-controlled phase 2 study. *Lancet* **2016**, *387*, 679–690.

(20) Armstrong, M. J.; Hull, D.; Guo, K.; Barton, D.; Hazlehurst, J. M.; Gathercole, L. L.; Nasiri, M.; Yu, J.; Gough, S. C.; Newsome, P. N.; Tomlinson, J. W. Glucagon-like peptide 1 decreases lipotoxicity in non-alcoholic steatohepatitis. *J. Hepatol.* **2016**, *64*, 399–408.

(21) Ivory, C. P.; Wallace, L. E.; McCafferty, D. M.; Sigalet, D. L. Interleukin-10-independent anti-inflammatory actions of glucagon-like peptide 2. *Am. J. Physiol Gastrointest Liver Physiol* **2008**, *295*, G1202–1210.

(22) El-Jamal, N.; Erdual, E.; Neunlist, M.; Koriche, D.; Dubuquoy, C.; Maggiotto, F.; Chevalier, J.; Berrebi, D.; Dubuquoy, L.; Boulanger, E.; Cortot, A.; Desreumaux, P. Glucagon-like peptide-2: broad receptor expression, limited therapeutic effect on intestinal inflammation and novel role in liver regeneration. *Am. J. Physiol Gastrointest Liver Physiol* **2014**, *307*, G274–285.

(23) Schaap, F. G.; Trauner, M.; Jansen, P. L. Bile acid receptors as targets for drug development. *Nat. Rev. Gastroenterol. Hepatol.* **2014**, *11*, 55–67.

(24) Yuan, L.; Bambha, K. Bile acid receptors and nonalcoholic fatty liver disease. *World J. Hepatol* **2015**, *7*, 2811–2818.

(25) Jeppesen, P. B.; Sanguinetti, E. L.; Buchman, A.; Howard, L.; Scolapio, J. S.; Ziegler, T. R.; Gregory, J.; Tappenden, K. A.; Holst, J.; Mortensen, P. B. Teduglutide (ALX-0600), a dipeptidyl peptidase IV resistant glucagon-like peptide 2 analogue, improves intestinal function in short bowel syndrome patients. *Gut* **2005**, *54*, 1224–1231.

(26) Schwartz, L. K.; O'Keefe, S. J.; Fujioka, K.; Gabe, S. M.; Lamprecht, G.; Pape, U. F.; Li, B.; Youssef, N. N.; Jeppesen, P. B. Long-term teduglutide for the treatment of patients with intestinal failure associated with short bowel syndrome. *Clin. Transl. Gastroenterol.* **2016**, *7*, e142.

(27) Pols, T. W.; Nomura, M.; Harach, T.; Lo Sasso, G.; Oosterveer, M. H.; Thomas, C.; Rizzo, G.; Gioiello, A.; Adorini, L.; Pellicciari, R.; Auwerx, J.; Schoonjans, K. TGR5 activation inhibits atherosclerosis by reducing macrophage inflammation and lipid loading. *Cell Metab.* **2011**, *14*, 747–757.

(28) Wang, Y. D.; Chen, W. D.; Yu, D.; Forman, B. M.; Huang, W. The G-protein-coupled bile acid receptor, Gpbar1 (TGR5), negatively regulates hepatic inflammatory response through antagonizing nuclear factor kappa light-chain enhancer of activated B cells (NF-kappaB) in mice. *Hepatology* **2011**, *54*, 1421–1432.

(29) Yoneno, K.; Hisamatsu, T.; Shimamura, K.; Kamada, N.; Ichikawa, R.; Kitazume, M. T.; Mori, M.; Uo, M.; Namikawa, Y.; Matsuoka, K.; Sato, T.; Koganei, K.; Sugita, A.; Kanai, T.; Hibi, T. TGR5 signalling inhibits the production of pro-inflammatory cytokines by in vitro differentiated inflammatory and intestinal macrophages in Crohn's disease. *Immunology* **2013**, *139*, 19–29.

(30) Cipriani, S.; Mencarelli, A.; Chini, M. G.; Distrutti, E.; Renga, B.; Bifulco, G.; Baldelli, F.; Donini, A.; Fiorucci, S. The bile acid receptor GPBAR-1 (TGR5) modulates integrity of intestinal barrier and immune response to experimental colitis. *PLoS One* **2011**, *6*, e25637.

(31) Sakanaka, T.; Inoue, T.; Yorifuji, N.; Iguchi, M.; Fujiwara, K.; Narabayashi, K.; Kakimoto, K.; Nouda, S.; Okada, T.; Kuramoto, T.; Ishida, K.; Abe, Y.; Takeuchi, T.; Umegaki, E.; Akiba, Y.; Kaunitz, J. D.; Higuchi, K. The effects of a TGR5 agonist and a dipeptidyl peptidase IV inhibitor on dextran sulfate sodium-induced colitis in mice. *J. Gastroenterol. Hepatol.* **2015**, *30* (Suppl1), 60–65.

(32) Hanauer, S. B. Inflammatory bowel disease: epidemiology, pathogenesis, and therapeutic opportunities. *Inflamm Bowel Dis* **2006**, *12* (Suppl 1), S3–9.

(33) Li, T.; Holmstrom, S. R.; Kir, S.; Umetani, M.; Schmidt, D. R.; Kliewer, S. A.; Mangelsdorf, D. J. The G protein-coupled bile acid receptor, TGR5, stimulates gallbladder filling. *Mol. Endocrinol.* **2011**, *25*, 1066–1071.

(34) Keitel, V.; Cupisti, K.; Ullmer, C.; Knoefel, W. T.; Kubitz, R.; Haussinger, D. The membrane-bound bile acid receptor TGR5 is localized in the epithelium of human gallbladders. *Hepatology* **2009**, *50*, 861–870.

(35) Briere, D. A.; Ruan, X.; Cheng, C. C.; Siesky, A. M.; Fitch, T. E.; Dominguez, C.; Sanfeliciano, S. G.; Montero, C.; Suen, C. S.; Xu, Y.; Coskun, T.; Michael, M. D. Novel small molecule agonist of TGR5 possesses anti-diabetic effects but causes gallbladder filling in mice. *PLoS One* **2015**, *10*, e0136873.

(36) Piotrowski, D. W.; Futatsugi, K.; Warmus, J. S.; Orr, S. T.; Freeman-Cook, K. D.; Londregan, A. T.; Wei, L.; Jennings, S. M.; Herr, M.; Coffey, S. B.; Jiao, W.; Storer, G.; Hepworth, D.; Wang, J.; Lavergne, S. Y.; Chin, J. E.; Hadcock, J. R.; Brenner, M. B.; Wolford, A. C.; Janssen, A. M.; Roush, N. S.; Buxton, J.; Hinchey, T.; Kalgutkar, A. S.; Sharma, R.; Flynn, D. A. Identification of tetrahydropyrido[4,3-d]pyrimidine amides as a new class of orally bioavailable TGR5 agonists. *ACS Med. Chem. Lett.* **2013**, *4*, 63–68.

(37) Phillips, D. P.; Gao, W.; Yang, Y.; Zhang, G.; Lerario, I. K.; Lau, T. L.; Jiang, J.; Wang, X.; Nguyen, D. G.; Bhat, B. G.; Trotter, C.; Sullivan, H.; Welzel, G.; Landry, J.; Chen, Y.; Joseph, S. B.; Li, C.; Gordon, W. P.; Richmond, W.; Johnson, K.; Bretz, A.; Bursulaya, B.; Pan, S.; McNamara, P.; Seidel, H. M. Discovery of trifluoromethyl-(pyrimidin-2-yl)azetidione-2-carboxamides as potent, orally bioavailable TGR5 (GPBAR1) agonists: structure-activity relationships, lead optimization, and chronic in vivo efficacy. *J. Med. Chem.* **2014**, *57*, 3263–3282.

(38) Cao, H.; Chen, Z. X.; Wang, K.; Ning, M. M.; Zou, Q. A.; Feng, Y.; Ye, Y. L.; Leng, Y.; Shen, J. H. Intestinally-targeted TGR5 agonists equipped with quaternary ammonium have an improved hypoglycemic effect and reduced gallbladder filling effect. *Sci. Rep.* **2016**, *6*, 28676.

(39) Duan, H.; Ning, M.; Zou, Q.; Ye, Y.; Feng, Y.; Zhang, L.; Leng, Y.; Shen, J. Discovery of intestinal targeted TGR5 agonists for the treatment of type 2 diabetes. *J. Med. Chem.* **2015**, *58*, 3315–3328.

(40) Ma, S. Y.; Ning, M. M.; Zou, Q. A.; Feng, Y.; Ye, Y. L.; Shen, J. H.; Leng, Y. OL3, a novel low-absorbed TGR5 agonist with reduced side effects, lowered blood glucose via dual actions on TGR5 activation and DPP-4 inhibition. *Acta Pharmacol. Sin.* **2016**, *37*, 1359.

(41) Filipinski, K. J.; Varma, M. V.; El-Kattan, A. F.; Ambler, C. M.; Ruggeri, R. B.; Goosen, T. C.; Cameron, K. O. Intestinal targeting of drugs: rational design approaches and challenges. *Curr. Top. Med. Chem.* **2013**, *13*, 776–802.

(42) Budzik, B. W.; Evans, K. A.; Wisnoski, D. D.; Jin, J.; Rivero, R. A.; Szewczyk, G. R.; Jayawickreme, C.; Moncol, D. L.; Yu, H. Synthesis and structure-activity relationships of a series of 3-aryl-4-isoxazolecarboxamides as a new class of TGR5 agonists. *Bioorg. Med. Chem. Lett.* **2010**, *20*, 1363–1367.

(43) Martin, R. E.; Bissantz, C.; Gavelle, O.; Kuratli, C.; Dehmlow, H.; Richter, H. G.; Obst Sander, U.; Erickson, S. D.; Kim, K.; Pietranico-Cole, S. L.; Alvarez-Sanchez, R.; Ullmer, C. 2-Phenoxy-nicotinamides are potent agonists at the bile acid receptor GPBAR1 (TGR5). *ChemMedChem* **2013**, *8*, 569–576.

(44) Ito, F.; Heard, N.; Kobayashi, H.; Kanzaki, N. Receptor agonist (Example 165, CAS# 878292–18–3). JP2006063064, 2006. Available from: <https://patentscope.wipo.int/search/en/detail.jsf?docId=JP22422972>. Accessed on February 19, 2018.

(45) Galia, E.; Nicolaidis, E.; Horter, D.; Lobenberg, R.; Reppas, C.; Dressman, J. B. Evaluation of various dissolution media for predicting in vivo performance of class I and II drugs. *Pharm. Res.* **1998**, *15*, 698–705.

(46) Ritchie, T. J.; Macdonald, S. J. The impact of aromatic ring count on compound developability—are too many aromatic rings a liability in drug design? *Drug Discovery Today* **2009**, *14*, 1011–1020.

(47) Lipinski, C. A.; Lombardo, F.; Dominy, B. W.; Feeney, P. J. Experimental and computational approaches to estimate solubility and permeability in drug discovery and development settings. *Adv. Drug Delivery Rev.* **2001**, *46*, 3–26.

(48) Charmot, D. Non-systemic drugs: a critical review. *Curr. Pharm. Des.* **2012**, *18*, 1434–1445.

(49) Rais, R.; Acharya, C.; Mackerell, A. D.; Polli, J. E. Structural determinants for transport across the intestinal bile acid transporter using C-24 bile acid conjugates. *Mol. Pharmaceutics* **2010**, *7*, 2240–2254.

(50) Maloney, P. R.; Parks, D. J.; Haffner, C. D.; Fivush, A. M.; Chandra, G.; Plunket, K. D.; Creech, K. L.; Moore, L. B.; Wilson, J. G.; Lewis, M. C.; Jones, S. A.; Willson, T. M. Identification of a chemical tool for the orphan nuclear receptor FXR. *J. Med. Chem.* **2000**, *43*, 2971–2974.

(51) Craddock, A. L.; Love, M. W.; Daniel, R. W.; Kirby, L. C.; Walters, H. C.; Wong, M. H.; Dawson, P. A. Expression and transport properties of the human ileal and renal sodium-dependent bile acid transporter. *Am. J. Physiol.* **1998**, *274*, G157–169.

(52) Surwit, R. S.; Kuhn, C. M.; Cochrane, C.; McCubbin, J. A.; Feinglos, M. N. Diet-induced type II diabetes in C57BL/6J mice. *Diabetes* **1988**, *37*, 1163–1167.

(53) Hubert, J.; Nawrocki, A.; Trujillo, M.; Powles, M.; Ormes, J.; Kurukulasuriya, R.; Dellurefic, J.; Shah, S. K.; Fung, S.; Wang, B.; Szezewyk, J.; Ravi, P.; Nargund, R. P.; Marsh, D. J.; Devita, R. J.; Poci, A. GPBAR1 agonism improves glucose metabolism and decreases gallbladder emptying in mice. *ADA Annual Meeting 2011*, abstract number 1003-P.

(54) Guimaraes, C. R.; Mathiowetz, A. M.; Shalaeva, M.; Goetz, G.; Liras, S. Use of 3D properties to characterize beyond rule-of-5 property space for passive permeation. *J. Chem. Inf. Model.* **2012**, *52*, 882–890.

(55) Lavoie, B.; Balemba, O. B.; Godfrey, C.; Watson, C. A.; Vassileva, G.; Corvera, C. U.; Nelson, M. T.; Mawe, G. M. Hydrophobic bile salts inhibit gallbladder smooth muscle function via stimulation of GPBAR1 receptors and activation of KATP channels. *J. Physiol.* **2010**, *588*, 3295–3305.

(56) Yusta, B.; Matthews, D.; Flock, G. B.; Ussher, J. R.; Lavoie, B.; Mawe, G. M.; Drucker, D. J. Glucagon-like peptide-2 promotes gallbladder refilling via a TGR5-independent, GLP-2R-dependent pathway. *Mol. Metab.* **2017**, *6*, 503–511.

(57) Kolossváry, I.; Guida, W. Low Mode Search. An efficient, automated computational method for conformational analysis: Application to cyclic and acyclic alkanes and cyclic peptides. *J. Am. Chem. Soc.* **1996**, *118*, 5011–5019.

(58) Labute, P. LowModeMD—implicit low-mode velocity filtering applied to conformational search of macrocycles and protein loops. *J. Chem. Inf. Model.* **2010**, *50*, 792–800.

(59) Labute, P.; Williams, C.; Feher, M.; Sourial, E.; Schmidt, J. M. Flexible alignment of small molecules. *J. Med. Chem.* **2001**, *44*, 1483–1490.